

Pseudogap and singlet formation in cuprate and organic superconductors

J. Merino¹ and O. Gunnarsson²

¹ *Departamento de Física Teórica de la Materia Condensada,
Condensed Matter Physics Center (IFIMAC) and Instituto Nicolás Cabrera,
Universidad Autónoma de Madrid, Madrid 28049, Spain*

² *Max-Planck-Institut für Festkörperforschung, Heisenbergstrasse 1, D-70569 Stuttgart, Germany*
(Dated: July 3, 2021)

The pseudogap phase occurring in cuprate and organic superconductors is analyzed based on the dynamical cluster approximation (DCA) approach to the Hubbard model. In this method a cluster embedded in a self-consistent bath is studied. With increasing Coulomb repulsion, U , the antinodal point [$\mathbf{k} = (\pi, 0)$] displays a gradual suppression of spectral density of states around the Fermi energy which is not observed at the nodal point [$\mathbf{k} = (\pi/2, \pi/2)$]. The opening of the antinodal pseudogap is found to be related to the internal structure of the cluster and the much weaker bath-cluster couplings at the antinodal than nodal point. The role played by internal cluster correlations is elucidated from a simple four-level model. For small U , the cluster levels form Kondo singlets with their baths leading to a peak in the spectral density. As U is increased a localized state is formed localizing the electrons in the cluster. If this cluster localized state is non-degenerate, the Kondo effect is destroyed and a pseudogap opens up in the spectra at the anti-nodal point. The pseudogap can be understood in terms of destructive interference between different paths for electrons hopping between the cluster and the bath. However, electrons at the nodal points remain in Kondo states up to larger U since they are more strongly coupled to the bath. The strong correlation between the $(\pi, 0)$ and $(0, \pi)$ cluster levels in the localized state leads to a large correlation energy gain which is important for localizing electrons and opening up a pseudogap at the anti-nodal point. Such scenario is in contrast with two independent Mott transitions found in two-band systems with different bandwidths in which the localized cluster electron does not correlate strongly with any other cluster electron for intermediate U . The important intracluster sector correlations are associated with the resonating valence bond (RVB) character of the cluster ground state containing d -wave singlet pairs. The low energy excitations determining the pseudogap have suppressed d -wave pairing indicating that the pseudogap can be related to breaking very short-range d -wave pairs. Geometrical frustration on the anisotropic triangular lattice relevant to κ -(BEDT-TTF)₂X leads to a switch in the character of the ground state of the cluster at intermediate hopping ratios $t'/t \sim 0.7$. Electron doping of the frustrated square lattice destroys the pseudogap in agreement with photoemission experiments on cuprates, due to a larger Schrieffer-Wolff exchange coupling, J_K , and a stronger cluster-bath coupling for the antinodal point.

PACS numbers: 71.30.+h; 71.27.+a; 71.10.Fd

I. INTRODUCTION

Cuprate and organic superconductors show a pseudogap in their phase diagram over a substantial temperature and doping range. The pseudogap shows up as a suppression of the many-body density of states at the Fermi energy in a number of experiments. For hole-doped cuprates this shows up as a dip in the photoemission spectrum in the $\mathbf{k} = (\pi, 0)$ direction, while there is a peak in the $\mathbf{k} = (\pi/2, \pi/2)$ direction.¹ The precise origin of the pseudogap is still a topic of debate. The understanding of the pseudogap is believed to be important for the electronic properties of cuprates, in particular, the mechanism of high- T_c superconductivity.

Both cuprates and the organic layered superconductors κ -(BEDT-TTF)₂X are strongly correlated two-dimensional systems, which are Mott^{2,3} insulators or close to Mott insulators. For the cuprates a square lattice is used and for the organics an anisotropic triangular lattice which are described by nearest neighbor and next-nearest-neighbor hopping. Undoped cuprates are antiferromagnetic insulators, driven by a large Coulomb

interaction U . Under doping the cuprates become metallic and the pseudogap is observed at small dopings in the underdoped range. On the other hand, the organics are half-filled Mott insulators at ambient pressure. These systems, which have weaker Coulomb repulsion than the cuprates, become metallic under hydrostatic pressure or by substitution of the anions X . Thereby the lattice parameter in the planes and the geometrical frustration can be varied. Hence, the cuprates are benchmark systems to analyze the doping-driven Mott transition whereas the organics are ideal examples of the Coulomb-driven Mott transition.

Early observation of the pseudogap in cuprates were made in, e.g., spin-lattice relaxation times,⁴ Knight shifts,⁵ resistivity,⁶ photoemission spectra,¹ Raman scattering,⁷ tunneling⁸ and scanning tunneling microscopy data.⁹ For a review see Timusk and Statt.¹⁰ Evidence of a pseudogap in metallic κ -(BEDT-TTF)₂X salts close to an antiferromagnetic Mott insulator comes from the T -dependence of magnetic susceptibility, $\chi(T)$, NMR relaxation rate, $\frac{1}{T_1 T}$ and Knight shift, $K(T)$ experiments.¹¹ A significant decrease in $\chi(T)$ is ob-

served below 50 K becoming steeper as the Mott transition is approached.¹² For instance, ^{13}C NMR $\frac{1}{T_1T}$ and $K(T)$ experiments¹³ on $\kappa\text{-(ET)}_2\text{Cu}[\text{N}(\text{CN})_2]\text{Br}$ display a suppression also below about 50 K becoming more pronounced in deuterated samples which are effectively closer to the Mott transition. Under hydrostatic pressures of 4 Kbar, $\frac{1}{T_1T}$ becomes nearly constant reestablishing conventional metallic behavior and no pseudogap. Metallic states obtained from the spin liquid¹⁴ Mott insulator, $\kappa\text{-(ET)}_2\text{Cu}_2(\text{CN})_3$ under pressures¹⁵ above 0.4 GPa do not show signs of a pseudogap in $\frac{1}{T_1T}$ experiments.

Despite their similarities¹⁶ there are also differences between cuprates and organics, doping being the crucial tuning parameter for cuprates and frustration and lattice parameter for the organics. Nevertheless, the pseudogap phenomenon appears similar in both types of systems, and closely related models are used to describe them. We will therefore address both classes of systems here.

There have been a large number of theories addressing the pseudogap in cuprates. Calculations based on the t - J model, the Dynamical Mean-Field Theory (DMFT) and the non-crossing approximation obtained a pseudogap in the local spectral function and related it to antiferromagnetic fluctuations.¹⁷ Calculations using embedded cluster methods,¹⁸ e.g., the dynamical cluster approximation (DCA), have reproduced a \mathbf{k} -dependent pseudogap for the Hubbard model of cuprates.^{19–25} The pseudogap was interpreted in terms of antiferromagnetic correlations,^{20,21} a momentum selective metal insulator transition^{22,23} or a low-frequency collective mode.²⁴ There has been much work relating the pseudogap to preformed superconducting pairs,^{26–29} which have not reached phase coherence and superconductivity at the temperature T and doping studied. On the other hand it has been argued that the pseudogap and superconductivity phases compete.³⁰

In the context of the $\kappa\text{-(BEDT-TTF)}_2\text{X}$ organics, there have been Path Integral Renormalization Group (PIRG),^{31,32} variational cluster perturbation theory,³³ cluster DMFT,^{34–36} finite- T Lanczos diagonalization³⁷ and cluster perturbation theory calculations³⁸ on the Hubbard model on an anisotropic triangular lattice. DMFT^{39–41} has been very successful in describing the crossover from a Fermi liquid to a 'bad' metal at low temperature, T^* , observed in resistivity,^{42,43} optical conductivity,⁴⁴ ultrasonic attenuation⁴⁵ and thermopower^{42,46} of $\kappa\text{-(BEDT-TTF)}_2\text{X}$. A pseudogap was found,^{34,38} from CDMFT on four site clusters and assigned to antiferromagnetic fluctuations.³⁸ The relevance of short range spin fluctuations to the pseudogap phase in organics has been discussed.⁴⁷ Cluster DMFT calculations show a reentrant behavior^{35,36,48} for the metal-insulator transition in agreement with experiment.⁴⁹ Several^{19,21,24,25,34–36,50,51} of the embedded cluster calculations have used clusters with four or fewer sites, which complicates the discussion of the large differences between $\mathbf{k} = (\pi, 0)$ and $(\pi/2, \pi/2)$, since the latter \mathbf{k} -vector

is not present for most of these small clusters and interpolation procedures have been used.

The dynamical cluster approximation (DCA) treats a cluster of N_c atoms embedded in a self-consistent bath. In much of the discussions, we describe the cluster in terms of the N_c one-particle levels with different \mathbf{K} vectors, where each state couples to its own bath. We perform numerical experiments to identify important factors for the pseudogap. We show that for, e.g., a $N_c = 8$ cluster, a pseudogap is formed also for a non self-consistent (metallic) bath. In contrast a non self-consistent DMFT ($N_c = 1$) calculation always gives a Kondo peak for a metallic bath. This shows the importance of the internal structure of the cluster. In a second numerical experiment, we exchange the baths for the $(\pi, 0)$ and $(0, \pi)$ cluster levels with the $(\pm\pi/2, \pm\pi/2)$ levels. The pseudogap then appears at $(\pi/2, \pi/2)$ instead of $(\pi, 0)$. This shows that the bath also plays a crucial role. The essential aspect is that the coupling to the $\mathbf{K} = (\pi, 0)$ and $(0, \pi)$ levels is much weaker than the coupling to the $(\pm\pi/2, \pm\pi/2)$ levels. The coupling to the bath of a \mathbf{K} -point is related to the second moment of the one-particle eigenvalue in a patch around the \mathbf{K} -point. This is much larger for the $(\pm\pi/2, \pm\pi/2)$ levels than for the $(\pi, 0)$ and $(0, \pi)$ levels.

Guided by a small ($N_c = 4$) cluster, giving a pseudogap, we construct a very simple four-level model, with two cluster levels each coupling to one bath level. The two cluster levels represent the $(\pi, 0)$ and $(0, \pi)$ \mathbf{K} -levels on the cluster. For a small Coulomb interaction U , the cluster levels form Kondo-like states with the bath. As U is increased, a localized state is formed on the cluster. If this localized state is nondegenerate, the Kondo-like states are destroyed and a pseudogap is formed. If the localized cluster state instead is a triplet, a new Kondo state is formed with the bath as U is increased and there is no pseudogap for moderate values of U . We analyze the formation of a pseudogap or a Kondo-like peak in terms of interference effects. By comparing correlation functions, we find that a $N_c = 8$ DCA calculation behaves in a similar way as the case with a localized nondegenerate cluster state. We emphasize the importance of the internal structure of the cluster. This leads to a competition between Kondo-like effects and the formation of a localized state on the cluster. Let us consider a $N_c = 8$ calculation with both $(\pi, 0)$, $(0, \pi)$ and $(\pm\pi/2, \pm\pi/2)$ cluster levels. For a small value of U , electrons in these levels form Kondo-like states with their baths. Electrons in the different cluster levels are only moderately correlated. As U is increased, the energy gain from the Kondo-like coupling is reduced and it becomes favorable to localize electrons in the $(\pi, 0)$ and $(0, \pi)$ cluster levels. This process, however, differs in essential ways from two independent Mott transitions in the two channels, as described in the dynamical mean-field theory (DMFT). Electrons in the $(\pi, 0)$ and $(0, \pi)$ levels become strongly correlated, in a similar way as for an isolated four site cluster. The corresponding energy gain is important for

driving the transition. The coupling to the bath is much larger for the $(\pm\pi/2, \pm\pi/2)$ than for the $(\pi, 0)$ and $(0, \pi)$ levels. The $(\pm\pi/2, \pm\pi/2)$ electrons therefore remain in Kondo-like states up to larger values of U . As U is increased further, it becomes favorable to also localize the $(\pm\pi/2, \pm\pi/2)$ electrons. All the electrons in the different cluster levels then become strongly correlated, leading to a large contribution to the energy. We also show why the pseudogap is lost for a frustrated electron-doped cuprate.

Very similar work has been done by Ferrero *et al.*,⁵² De Leo *et al.*,⁵⁰ and Capone *et al.*,⁵³ who considered two- and three-orbital Anderson models and a four-impurity model. This work emphasized the interorbital interaction and the cross over from a Kondo screened state to an unscreened state. The work mainly addressed A_3C_{60} ($A = K, Rb$) and did not address the \mathbf{k} dependence of the pseudogap for the cuprates.

The work presented here is an in-depth extension of our previous short paper⁵⁴ and is organized as follows. In Sec. II we introduce the Hubbard model relevant to the cuprates and organics and summarize key aspects of the DCA method. In Sec. III we show general aspects of the model obtained within DCA such as spin and pairing correlations, double occupancies and phase diagram. We discuss how the pseudogap observed close to the Mott transition is already present in the quantum impurity problem even without the self-consistency condition. This allows us to concentrate on first iteration results. Some general features of the spectra are found already in a two-level model presented in Sec. IV. To obtain a pseudogap, however, we have to introduce a four-level model in Sec. V. We present an explanation of the pseudogap in terms of destructive interference in Sec. VI. This analysis is extended in Sec. VII to understanding the pseudogap in $N_c = 8$ clusters which contain both $(\pi, 0)$ and $(\pi/2, \pi/2)$ sectors. We compare correlation functions to show that the $N_c = 8$ DCA calculation behaves in a similar way as the four-level model. We also analyze the evolution of the pseudogap with geometrical frustration and doping relevant to the cuprates. The character and implications of the pseudogap found within quantum cluster theories are discussed in Secs. VIII and IX.

II. MODEL AND METHOD

A minimal model for understanding the properties of layered organic compounds or cuprates is a Hubbard model on a two-dimensional lattice

$$H = t \sum_{\langle ij \rangle, \sigma} (c_{i\sigma}^\dagger c_{j\sigma} + c_{j\sigma}^\dagger c_{i\sigma}) + t' \sum_{\langle\langle ij \rangle\rangle, \sigma} (c_{i\sigma}^\dagger c_{j\sigma} + c_{j\sigma}^\dagger c_{i\sigma}) + U \sum_i n_{i\uparrow} n_{i\downarrow} - \mu \sum_{i\sigma} c_{i\sigma}^\dagger c_{i\sigma} \quad , \quad (1)$$

where σ is the spin index, U is an on-site Coulomb interaction, t describes the nearest neighbor $\langle\langle ij \rangle\rangle$ hopping and t' the second nearest neighbor hopping $\langle\langle\langle ij \rangle\rangle\rangle$.

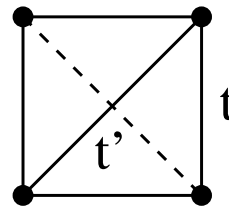


FIG. 1. Hopping integrals for the Hubbard model. For cuprates the hopping integral t' along both diagonals (full and dashed lines) are included (square lattice), while for the organics only the hopping along one diagonal (full line) is included (triangular lattice).

These hoppings are shown in Fig. 1. For the cuprates we use hopping along both diagonals with $t'/t \leq 0$ ("square lattice") and for organics hopping along one diagonal with $t'/t \geq 0$ ("triangular lattice"). The hole creation and destruction operators are given by $c_{i\sigma}^\dagger$ and $c_{i\sigma}$. We fix $t = -0.04$ eV which is the appropriate value for describing the lowest energy band arising from the antibonding orbitals of the dimerized molecules in organic materials.⁵⁵ For the cuprates $t = -0.4$ eV is more appropriate.⁵⁶ We vary U and the t'/t ratio. All units are given in eV unless explicitly stated.

The Coulomb part of the Hamiltonian is rewritten as

$$U \sum_i n_{i\uparrow} n_{i\downarrow} = U \sum_i (n_{i\uparrow} - n_0)(n_{i\downarrow} - n_0) \quad (2) + U n_0 \sum_{i\sigma} n_{i\sigma} - U \sum_i n_0^2,$$

where n_0 may be chosen as $n/2$, where n is the average occupancy. The first term in Eq. (2) is the new many-body term, while the second term is a one-body term. In the limit of a small U , the Hartree-Fock self-energy, $\Sigma_{i\sigma}^{\text{HF}} = U \langle n_{i-\sigma} \rangle$, is a good approximation to the self-energy $\Sigma_{i\sigma}$. $U n_0$, with $n_0 = n/2$, is then an approximation to the self-energy, and the remaining part of the self-energy, $\Sigma_c \equiv \Sigma - \Sigma^{\text{HF}}$ below, is reduced. With this choice Σ_c goes to zero as the frequency goes to infinity.

The model above is solved using the dynamical cluster approximation (DCA).¹⁸ Here we summarize the main steps in the theory. The Brillouin zone is divided into N_c patches denoted by the momenta \mathbf{K} , at each patch center. The \mathbf{k} vectors of a patch are given by $\mathbf{K} + \tilde{\mathbf{k}}$, where $\tilde{\mathbf{k}}$ can run over a finite but large number of points. The problem is reduced to solving a cluster embedded in an effective bath. The bath is described by the cluster excluded Green's function $G_0(z)$, where G_0 is a $N_c \times N_c$ matrix. Solving the cluster in this bath gives a cluster Green's function G_c . From this a self-energy is extracted

$$\Sigma_c(z) = G_0^{-1}(z) - G_c^{-1}(z). \quad (3)$$

A coarse-grained Green's function is calculated

$$\bar{G}(z) = \frac{N_c}{N} \sum_{\tilde{\mathbf{k}}} \{ [G_0^0(\tilde{\mathbf{k}}, z)]^{-1} - \Sigma_c(z) \}^{-1}, \quad (4)$$

where $[G_0^0(\tilde{\mathbf{k}}, z)]_{\mathbf{K}, \mathbf{K}} = 1/(z - \Delta - \varepsilon_{\mathbf{K}+\tilde{\mathbf{k}}})$ is a free-electron Green's function,

$$\Delta = n_0 U - \mu \quad (5)$$

and N is the total number of $\mathbf{K} + \tilde{\mathbf{k}}$ -points. A new bath Green's function is extracted

$$G_0(z) = [\bar{G}^{-1}(z) + \Sigma_c(z)]^{-1}, \quad (6)$$

and the approach is iterated to self-consistency. Here we mainly study $N_c = 4, 8$ and 16 . We use the clusters of Betts *et al.*⁵⁷ For instance we use clusters 8A and 16B in their notations. Here we use a spin independent G_0 .

The bath Green's function can also be written as

$$G_0(z) \equiv [z - \Delta - \bar{\varepsilon}_{\mathbf{K}} - \Gamma_{\mathbf{K}}(z)]^{-1}, \quad (7)$$

where $\bar{\varepsilon}_{\mathbf{K}} = (N_c/N) \sum_{\tilde{\mathbf{k}}} \varepsilon_{\mathbf{K}+\tilde{\mathbf{k}}}$. For the case of $\Sigma_c(z) \equiv 0$ we then obtain

$$\frac{N_c}{N} \sum_{\tilde{\mathbf{k}}} \frac{1}{z - \Delta - \varepsilon_{\mathbf{K}+\tilde{\mathbf{k}}}} = \frac{1}{z - \Delta - \bar{\varepsilon}_{\mathbf{K}} - \Gamma_{\mathbf{K}}(z)}. \quad (8)$$

We can obtain some additional understanding by expanding the left and right hand sides of Eq. (8) to second order in $1/z$. This leads to the sum rule⁵⁸

$$\frac{1}{\pi} \int \text{Im} \Gamma_{\mathbf{K}}(\varepsilon) d\varepsilon = \frac{N_c}{N} \sum_{\tilde{\mathbf{k}}} (\varepsilon_{\mathbf{K}+\tilde{\mathbf{k}}} - \bar{\varepsilon}_{\mathbf{K}})^2, \quad (9)$$

where $\Gamma_{\mathbf{K}}(i\omega_n)$ has been analytically continued to real ε . If the bath is described by a finite number of levels with the energies ε_i and couplings $V_{\mathbf{K}i}$ to the cluster state \mathbf{K} , $\Gamma_{\mathbf{K}}(\varepsilon) = \sum_i |V_{\mathbf{K}i}|^2 / (\varepsilon - \varepsilon_i)$ and the sum rule above is related to $\sum_i |V_{\mathbf{K}i}|^2$. This result shows that the second moment of the $\varepsilon_{\tilde{\mathbf{k}}}$ inside a patch is a measure of the coupling to the bath. Due to the weak dispersion around $\mathbf{K} = (\pi, 0)$, $\Gamma_{\mathbf{K}}(z)$ is much smaller than around $\mathbf{K} = (\pi/2, \pi/2)$. For $N_c = 8$ the difference is roughly a factor of three to four. This is illustrated in Fig. 2. This result is crucial for the following discussion. As is discussed in Sec. VII B 2 the coupling can also depend on the details of the density of states and the position of the chemical potential μ in a rather important way.

In the DCA procedure, the hopping integrals used in the embedded cluster differ from the ones in the Hubbard model in Eq. (1). For instance for the cluster 8A the nearest and second nearest hopping integrals are $t_{\text{cluster}} = 0.81t$ and $t'_{\text{cluster}} = 1.27t'$, respectively. For $N_c = 8$ second nearest neighbor sites are connected by a direct hopping as well as a hopping due to periodic boundary conditions. These two integrals are added in the DCA, which leads to the large prefactor 1.27. In the following, we discuss results in the DCA by performing calculations for isolated clusters. For these clusters we then use the rescaled values of the hopping parameters to be able to compare as closely as possible with the DCA results.

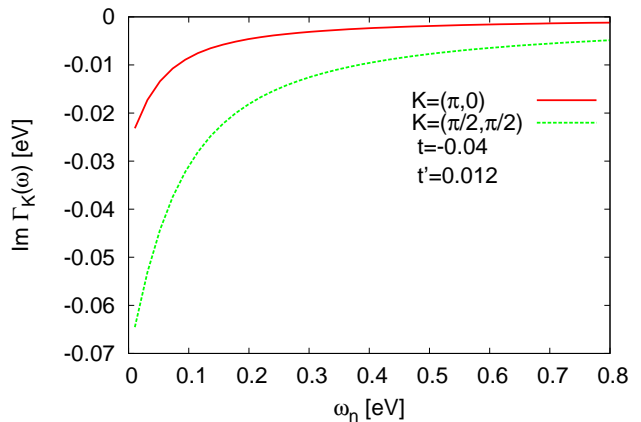


FIG. 2. Coupling $\Gamma_{\mathbf{K}}(i\omega_n)$ for $\mathbf{K} = (\pi, 0)$ and $(\pi/2, \pi/2)$ for $\Sigma_c(z) \equiv 0$. The parameters are $N_c = 8$, $t = -0.04$ eV, $t' = 0.012$ eV, $U = 0$ eV, $\mu = 0$ eV and $T = 38.4$ K. The figure illustrates how the coupling is much stronger for $\mathbf{K} = (\pi/2, \pi/2)$ than $(\pi, 0)$.

The Green's function can be written as

$$G(\mathbf{K}, \omega_n) = \frac{1}{i\omega_n + \mu - \varepsilon_{\mathbf{K}} - n_0 U - \Sigma_c(\mathbf{K}, \omega_n)}. \quad (10)$$

This form can be analytically continued to real frequencies using Maximum Entropy.⁵⁹ This provides a good approximation for the spectrum of the wave vector \mathbf{K} for the homogeneous system. In Sec. IX we deal with an inhomogeneous system. Then we Fourier transform the real space Green's function of the cluster to reciprocal space and obtain spectra of the cluster. For a homogeneous system this would correspond to averaging the spectrum over the patch surrounding a \mathbf{K} -point, which leads to a broader spectrum than Eq. (10).

For a small range of U and T values, both a metallic and insulating state can be obtained, depending on the state of the first iteration. In this case we have studied the metallic phase, unless explicitly stating the opposite. For large values of U the system supports an antiferromagnetic solution with a polarized bath. In these cases we have nevertheless used a paramagnetic bath.

III. RESULTS

In this section we present results of the properties of the Hubbard model within the DCA. In the following sections we will analyze and discuss the origin of the pseudogap in quantum cluster approaches.

A. Spin and pairing correlations

We introduce a pairing operator

$$\Delta_i^\dagger = \frac{1}{2} \sum_{\delta} f(\delta) c_{i\uparrow}^\dagger c_{i+\delta\downarrow}^\dagger, \quad (11)$$

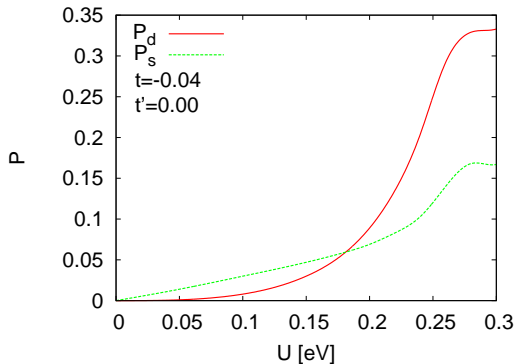


FIG. 3. (Color online) Dependence of pairing amplitudes P on the Coulomb repulsion, U , in the half-filled Hubbard model on a square lattice. Extended s -wave (dotted curve) and $d_{x^2-y^2}$ -wave (full curve) pairing channels are considered. The parameters are $t = -0.04$ eV, $t' = 0$ and $T = 38.4$ K, and the calculations are self-consistent.

where the sum over δ runs over the nearest neighbor lattice sites. If $i + \delta$ falls outside the cluster, it is periodically continued inside the cluster. The function $f(\delta)$ describes the symmetry of the pairing. We use $f(\pm 1, 0) = 1$ and $f(0, \pm 1) = 1$ for extended s -wave symmetry, $f(\pm 1, 0) = 1$ and $f(0, \pm 1) = -1$ for $d_{x^2-y^2}$ symmetry and $f(1, 1) = f(-1, -1) = 1$ and $f(1, -1) = f(-1, 1) = -1$ for d_{xy} symmetry. We then calculate

$$P = \frac{1}{N_c} \left(\sum_{ij} \langle \Delta_i^\dagger \Delta_j \rangle - \frac{1}{4} \sum_{ij\delta\gamma} f(\delta)f(\gamma) \langle c_{i\uparrow}^\dagger c_{j\uparrow} \rangle \langle c_{i+\delta\downarrow}^\dagger c_{j+\gamma\downarrow} \rangle \right), \quad (12)$$

where we have subtracted a term so that $P = 0$ for non-interacting electrons. Without the subtraction term and for small cluster, P can sometimes be large because of a large contribution for $i = j$. Since a tendency to superconductivity is indicated by substantial contributions from i and j far apart, it is desirable to reduce the importance of the contributions for $i = j$.

Fig. 3 shows a rapid increase in the $d_{x^2-y^2}$ channel as U is increased and the system approaches a Mott transition. This pairing channel wins over the extended s -wave channel for large values of U .

In Fig. 4 we show the longitudinal spin-spin correlation function of the electrons:

$$S(\mathbf{q}) = \frac{1}{N_c} \sum_{ij} e^{i\mathbf{q}\mathbf{R}_{ij}} \langle S_i^z S_j^z \rangle, \quad (13)$$

where $S_i^z = (n_{i\uparrow} - n_{i\downarrow})/2$ is the z -component of \mathbf{S}_i , which is evaluated at the antiferromagnetic ordering vector $\mathbf{Q} = (\pi, \pi)$.

We compare the results of the average value for $S(\mathbf{Q})$ obtained from DCA with the case in which we have perfect Néel order and the case of the pure RVB state which is the exact ground state of the Heisenberg model on the

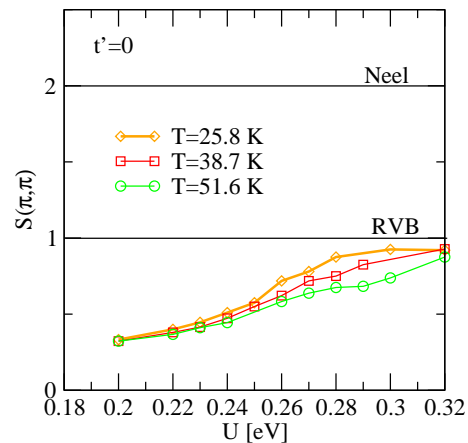


FIG. 4. (Color online) Magnetic correlations across the metal insulator transition from self-consistent DCA for $N_c = 8$. The dependence of the spin structure factor at (π, π) on U for $t' = 0$ is compared to a full antiferromagnetic Néel state and pure RVB states (marked with the horizontal lines). Self-consistent DCA calculations are shown. The figure shows how spin correlations obtained from DCA saturate at the value expected for the RVB state in the Mott insulating phase.

$N_c = 8$ cluster (see discussion in Sec. III B). The spin correlations are found to saturate to the RVB value as the Mott transition is approached. This value is $S(\pi, \pi) = 1$, which is half of the value that would be found for pure Néel states. At moderate U values before the Mott transition occurs the spin correlations are not quite saturated to the pure RVB state. For example, for $U = 0.25$ eV, within the pseudogap phase we find that $S(\pi, \pi) = 0.6$, still far from the pure spin liquid state value. In all cases we have considered a paramagnetic solution.

B. Sector correlation functions and RVB

We now analyze in detail the ground state properties of isolated clusters in order to gain insight in the predictions of DCA embedded cluster calculations. We perform a detailed comparison of the exact cluster properties with predictions from RVB theory.

1. Cluster correlations of the isolated cluster: unfrustrated case

The ground state can be characterized through the correlation functions between nodal $(\pm\pi/2, \pm\pi/2)$ and antinodal $(\pi, 0), (0, \pi)$ cluster \mathbf{K} -sectors

$$C_{\mathbf{K}\sigma, \mathbf{K}'\sigma'} = \langle n_{\mathbf{K}\sigma} n_{\mathbf{K}'\sigma'} \rangle - \langle n_{\mathbf{K}\sigma} \rangle \langle n_{\mathbf{K}'\sigma'} \rangle. \quad (14)$$

As we will see in Secs. V and VII, a positive correlation of $C_{\mathbf{K}\uparrow, \mathbf{K}\downarrow} > 0$ for $\mathbf{K} = (\pi/2, \pi/2)$ and $(\pi, 0)$ sectors is typically found at large U using the DCA for $t' = 0$. This corresponds to a localized state in the cluster

TABLE I. Correlations between $\mathbf{K} = (\pi, 0)$ and $\mathbf{K}' = (0, \pi)$ sectors obtained with ED on the isolated clusters of size N_c in the limit $U \gg |t|$ and $t' = 0$.

N_c	$C_{\mathbf{K}\uparrow, \mathbf{K}\downarrow}$	$C_{\mathbf{K}\uparrow, \mathbf{K}'\uparrow}$	$C_{\mathbf{K}\uparrow, \mathbf{K}'\downarrow}$
4	0.125	-0.166	-0.208
8	0.063	-0.125	-0.188
16	0.031	-0.093	-0.153

TABLE II. Correlations between $\mathbf{K} = (\pi/2, \pi/2)$ and $\mathbf{K}' = (-\pi/2, -\pi/2)$ sectors obtained with ED on the isolated clusters of size N_c in the large $U \gg |t|$ limit and $t' = 0$.

N_c	$C_{\mathbf{K}\uparrow, \mathbf{K}\downarrow}$	$C_{\mathbf{K}\uparrow, \mathbf{K}'\uparrow}$	$C_{\mathbf{K}\uparrow, \mathbf{K}'\downarrow}$
8	0.063	-0.125	-0.188
16	0.031	-0.093	-0.153

which correlates well with the opening of a gap in the \mathbf{K} -sector spectra at the Fermi surface. Increasing the cluster size, N_c , leads to a reduction of the sector correlations. In order to understand this behavior, we compare the exact ground state of the cluster with Anderson's RVB wavefunction. We show that the ground state of the $N_c = 4$ and 8 clusters is exactly described by a nearest-neighbor RVB (NN-RVB). This is also a very good approximation of the ground state of the $N_c = 16$ cluster.

Using the ED formulation we obtain the isolated cluster correlations between different sectors. The results for different cluster sizes are displayed in Tables I and II.

These correlations may be compared with results for the correlations using the NN-RVB wavefunction as introduced by Liang, Doucot and Anderson⁶⁰ for bipartite lattices. Such a wavefunction was introduced in the context of the $S = 1/2$ Heisenberg antiferromagnet on the square lattice ($t' = 0$) to compare to the exact singlet ground state. The NN-RVB is a superposition of singlets between neighboring sites taken from A to B sublattice with equal positive bond amplitudes:

$$|\Psi_0\rangle = \sum_{i_\alpha, j_\beta} (i_1 j_1)(i_2 j_2) \dots (i_n j_n) \quad (15)$$

where i_α (j_β) denote neighbor sites in the A-sublattice (B-sublattice) and $(i_\alpha j_\beta)$ denotes a singlet. Using this construction, the Marshall sign convention⁶¹ for the amplitude of ground state configurations in bipartite lattices is automatically satisfied. We restrict our analysis to the NN-RVB state avoiding the arbitrariness in the decay of singlet bond amplitudes with the relative distance.

The exact ground state of the Hubbard model on the $N_c = 4$ cluster for $U \gg t$ coincides with the⁶² NN-RVB

TABLE III. Correlations between $\mathbf{K} = (\pi, 0)$ and $\mathbf{K}' = (0, \pi)$ sectors obtained with the NN-RVB wavefunction on isolated clusters of size N_c .

N_c	$C_{\mathbf{K}\uparrow, \mathbf{K}\downarrow}$	$C_{\mathbf{K}\uparrow, \mathbf{K}'\uparrow}$	$C_{\mathbf{K}\uparrow, \mathbf{K}'\downarrow}$
4	0.125	-0.166	-0.208
8	0.063	-0.125	-0.188
16	0.031	-0.071	-0.111

TABLE IV. Correlations between $\mathbf{K} = (\pi/2, \pi/2)$ and $\mathbf{K}' = (-\pi/2, -\pi/2)$ sectors obtained with the NN-RVB on the isolated clusters of size N_c .

N_c	$C_{\mathbf{K}\uparrow, \mathbf{K}\downarrow}$	$C_{\mathbf{K}\uparrow, \mathbf{K}'\uparrow}$	$C_{\mathbf{K}\uparrow, \mathbf{K}'\downarrow}$
8	0.063	-0.125	-0.188
16	0.031	-0.071	-0.111

(Eq. 15):

$$\begin{aligned} |\Psi_0\rangle &= (12)(34) + (14)(32) \\ &= \frac{1}{\sqrt{3}} (|1\uparrow, 2\downarrow, 3\uparrow, 4\downarrow\rangle + |1\downarrow, 2\uparrow, 3\downarrow, 4\uparrow\rangle) \\ &\quad - \frac{1}{2\sqrt{3}} (|1\uparrow, 2\downarrow, 3\downarrow, 4\uparrow\rangle + |1\downarrow, 2\uparrow, 3\uparrow, 4\downarrow\rangle) \\ &\quad + |1\uparrow, 2\uparrow, 3\downarrow, 4\downarrow\rangle + |1\downarrow, 2\downarrow, 3\uparrow, 4\uparrow\rangle, \end{aligned} \quad (16)$$

where (12)(34) and (14)(32) describe the four site plaquettes factorized into horizontal and vertical singlets, respectively (with 1 and 3 being on a diagonal). In $N_c = 8$ clusters, all singlet bonds (ij) that can be formed between A and B sublattices are nearest neighbors so that the NN-RVB is also the exact ground state of this cluster.

The sector correlations obtained exactly on the different clusters at large U are shown in Tables I and II and the ones obtained using the NN-RVB are shown in Tables III and IV. The overlap between the NN-RVB, $|RVB\rangle$ and the ground state of the cluster is: $|\langle RVB|\Psi_0\rangle| = 1$ for $N_c = 4, 8$, and $|\langle RVB|\Psi_0\rangle| = 0.93$ for $N_c = 16$. This indicates that the ground states of the $N_c = 4$ and $N_c = 8$ clusters are pure short range RVB spin liquid states.⁶³ The correlations between different sectors of the ground state of the $N_c = 16$ cluster deviate somewhat from the pure NN-RVB wavefunction whereas the intrasector correlations for $N_c = 16$ agree with the NN-RVB state. The ground state of the $N_c = 16$ cluster is very close but does not exactly coincide with the NN-RVB spin liquid state. The differences may be attributed to neglecting more distant bonds in the bond factorization.

2. Ground state cluster properties in the thermodynamic limit for $t'=0$

In order to gain insight on the ground state properties of the cluster in the thermodynamic limit we have explored the pairing correlations on clusters of up to

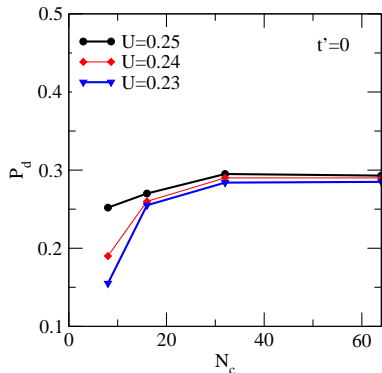


FIG. 5. (Color online) d -wave pairing correlations for different clusters from self-consistent DCA for $t' = 0$. The correlation length at $T = 38.4$ K can be obtained from the saturation of P_d .

$N_c = 64$ sites. The dependence of P_d with N_c as obtained from DCA is shown in Fig. 5 at fixed temperature $T = 38.4$ K and different U . P_d saturates with cluster size, meaning that there is only very short range correlation.

The behavior of AF spin correlations in large systems can be obtained from DCA calculations on the largest $N_c = 64$ site cluster we have considered. In Fig. 6 we show the dependence of $(-1)^{(r_x+r_y)}\langle S_i^z S_j^z \rangle$ between sites i and j at a relative distance: $\mathbf{r} = \mathbf{R}_i - \mathbf{R}_j$ inside the $N_c = 64$ cluster. The spin correlations are found to decay very slowly with the relative distance between sites, $|\mathbf{r}| = \sqrt{r_x^2 + r_y^2}$. Since the calculation is performed at low but finite temperatures Mermin-Wagner theorem predicts no long range order in the two-dimensional lattice. On the other hand, the slow decay observed is consistent with the long range order expected at $T = 0$ in the Heisenberg model on the square lattice in the thermodynamic limit.⁶⁴ This is also consistent with the need of including further distant singlet bonds between sites when describing the exact ground state correlations of clusters with $N_c > 8$ using RVB states discussed previously.⁶⁰

3. Cluster correlations on the isolated cluster: geometrical frustration effects

We now turn on the geometrical frustration, t'/t , which is present both for cuprate and organic superconductors. Here we focus on the organic superconductors with a triangular lattice. Below we perform calculations for isolated clusters to understand the results better. As discussed in Sec. II, in DCA the hopping integrals of the embedded cluster are rescaled from the values in the Hubbard model. Below we give the hoppings of the Hubbard model, t and t' . The corresponding hopping parameters for the cluster are then ($N_c = 8$ and cluster 8A according to Ref. 57) $t_{\text{cluster}} = 0.81t$ and $t'_{\text{cluster}} = 1.27t'$. These parameters are then also used for the isolated clus-

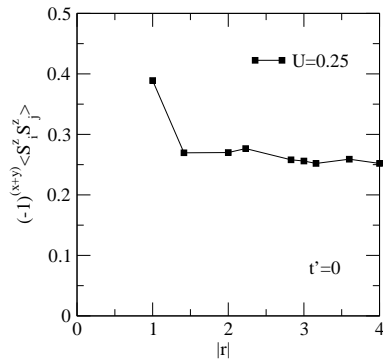


FIG. 6. (Color online) Decay of spin correlations with relative distance, $|\mathbf{r}|$, between sites i and j inside the $N_c = 64$ cluster for $t = -0.04$ eV and $t' = 0$ at $T = 38.4$ K in a self-consistent calculation.

TABLE V. Dependence of correlations between $\mathbf{K} = (\pi, 0)$ and $\mathbf{K}' = (0, \pi)$ for different t'/t from ED on $N_c = 8$ isolated clusters. The hopping $t_{\text{cluster}} = -0.0324$ ($t = -0.04$) eV and $U = 0.3$ eV are used in a triangular lattice model for organics.

t'/t	$C_{\mathbf{K}\uparrow, \mathbf{K}\downarrow}$	$C_{\mathbf{K}\uparrow, \mathbf{K}'\uparrow}$	$C_{\mathbf{K}\uparrow, \mathbf{K}'\downarrow}$
0	0.072	-0.131	-0.191
0.5	0.072	-0.131	-0.191
0.7	0.072	-0.131	-0.191
0.8	0.063	-0.012	0.032
1.	0.057	-0.0092	0.031

ter. We show in tables V and VI results for varying degree of geometrical frustration, t'/t . Apart from overall quantitative changes we find a qualitative change in $C_{(\pi/2, \pi/2)\uparrow, (-\pi/2, -\pi/2)\downarrow}$ which displays a positive correlation for $t'/t > 0.7$, instead of the negative correlation found for the unfrustrated case: $t' = 0$. A similar change is seen for $C_{(\pi, 0)\uparrow, (0, \pi)\downarrow}$.

In order to understand the origin of this sudden change of correlation functions we have explored pairing correlations. In table VII we show the dependence of pairing correlations on t'/t for a $N_c = 8$ cluster. The figure shows how the $d_{x^2-y^2}$ and extended- s pairing are strongly suppressed and the d_{xy} becomes positive and large at $t' \geq 0.7t$. The fact that at the same time $C_{(\pi/2, \pi/2)\uparrow, (-\pi/2, -\pi/2)\downarrow}$ becomes positive is a consequence of d_{xy} pairing since $C_{(\pi/2, \pi/2)\uparrow, (-\pi/2, -\pi/2)\downarrow}$ is related to the strength of pairing correlations at the nodal points. This sudden switch in the pairing and correlation functions occurs at a crossing of cluster states. A similar change from $d_{x^2-y^2}$ to d_{xy} has been found previously⁵⁰ in smaller $N_c = 4$ clusters on a frustrated square lattice.

To discuss the crossing of states in more detail, we show in Fig. 7 some low-lying states for different degree of geometrical frustration. For $t'/t < 0.7$ the occupancies of the $(\pi, 0)$, $(0, \pi)$ and $(\pm\pi/2, \pm\pi/2)$ orbitals are the same and equal to unity. The system uses these six orbitals to form a state where the Coulomb repulsion is strongly reduced. As t' is increased, the $(\pi/2, -\pi/2)$ and $(-\pi/2, \pi/2)$ or-

TABLE VI. Dependence of correlations between $\mathbf{K} = (\pi/2, \pi/2)$ and $\mathbf{K}' = (-\pi/2, -\pi/2)$ for different t'/t from ED on $N_c = 8$ isolated clusters. The hopping $t_{\text{cluster}} = -0.0324$ ($t = -0.04$) eV and $U = 0.3$ eV are used in a triangular lattice model for organics.

t'/t	$C_{\mathbf{K}\uparrow, \mathbf{K}\downarrow}$	$C_{\mathbf{K}\uparrow, \mathbf{K}'\uparrow}$	$C_{\mathbf{K}\uparrow, \mathbf{K}'\downarrow}$
0	0.072	-0.131	-0.191
0.5	0.072	-0.131	-0.191
0.7	0.072	-0.131	-0.191
0.8	0.048	-0.012	0.048
1.	0.044	-0.0092	0.044

TABLE VII. Dependence of pairing correlations with t'/t from ED on $N_c = 8$ isolated clusters with $t_{\text{cluster}} = -0.0324$ ($t = -0.04$) eV and $U = 0.3$ eV in the triangular lattice model for organics.

t'/t	P_s	$P_{d_{x^2-y^2}}$	$P_{d_{xy}}$
0	0.19	0.39	-0.5
0.5	0.19	0.39	-0.5
0.7	0.19	0.39	-0.5
0.8	0.014	-0.012	0.71
1.	0.015	-0.0092	0.65

bitals are lowered and the other orbitals in the space discussed above are raised. The occupancy of the orbitals, however, is such that the energy is unchanged. At $t'/t > 0.7$ this changes. The lowest state is now one where occupancy of $(\pi/2, -\pi/2)$ and $(-\pi/2, \pi/2)$ is substantially larger than unity (~ 1.5) and the occupancy of the orbitals which move upwards is reduced. The result is a more negative hopping energy. However, the system now has smaller possibilities to correlate the electrons, and the Coulomb repulsion is larger. For $t'/t > 0.7$ this is favorable. For instance, for $t'/t = 0.8$, the Coulomb energy is 0.093 (0.075) eV and the hopping energy is -0.216 (-0.186) eV for the lowest state (the state that was lowest for smaller t').

The lowest state is always non-degenerate, except around $t'/t = 0.7$, where levels cross. We will see below how the switch from a non-degenerate to a degenerate lowest cluster state, coupled to a metallic bath, can lead to a switch from a non-Kondo to a bath-cluster Kondo singlet formation. This is crucial for the pseudogap destruction and may play a role for its disappearance as the geometrical frustration is increased in the organics. However, this should be taken with caution since for $t' = t$ the (non-degenerate) ground-state in the cluster is again well separated from higher states, as can be observed in Fig. 7.

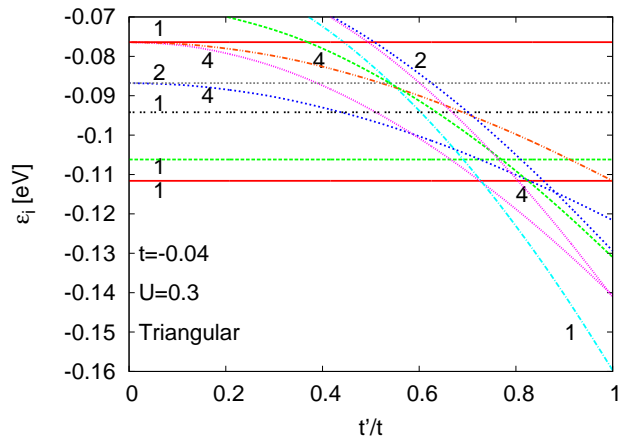


FIG. 7. Low-lying levels for an isolated, triangular cluster with $N_c = 8$ as a function of t'/t ($t'_{\text{cluster}}/t_{\text{cluster}} = 1.57t'/t$). The numbers show the level degeneracies. The Hubbard model parameters are $t = -0.04$ eV and $U = 0.3$ eV.

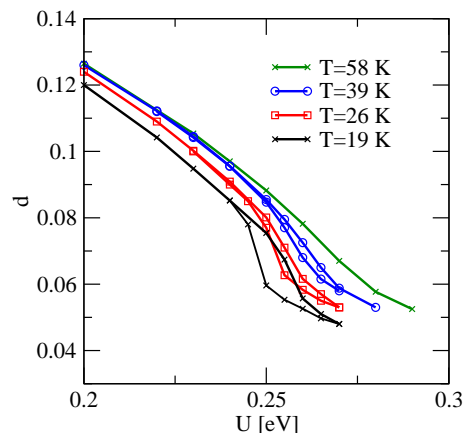


FIG. 8. (Color online) Dependence of double occupancy d on U in the half-filled Hubbard model on a square lattice. The parameters are $t = -0.04$ eV, $t' = 0$ and the calculations are self-consistent.

C. Double occupancy

The double occupancy d can be used as a measure of a metal-insulator transition.⁶⁵ The transition shows up as a rapid drop in d as a function of U at the transition. Fig. 8 shows the double occupancy for a nonfrustrated lattice. For large T there is just a smooth drop with U . For smaller T , however, the drop is much more rapid, signaling a metal-insulator transition. The curve $d(U)$ shows hysteresis. As U is increased, there is a strong drop at some $U_{c2}(T)$, where a metallic state cannot any longer be stabilized. As U is then decreased, there is a rapid increase at some $U_{c1}(T) < U_{c2}(T)$, where the insulating state cannot be stabilized. This kind of hysteresis is well-known from DMFT and DCA calculations.

Geometrical frustration can be varied by changing t'/t . In the left part of Fig. 9 we show the behavior of the

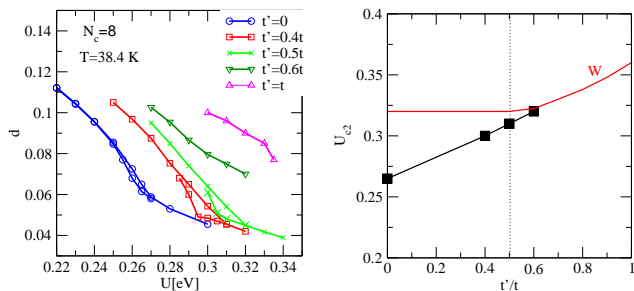


FIG. 9. (Color online) Dependence of double occupancy d on U and geometrical frustration for a triangular lattice from self-consistent DCA. An increase of the critical value U_{c2} is found with t'/t which is plotted in the right panel. This is compared with the dependence of the bare bandwidth W on t'/t . The bandwidth increases from $W = 0.32\text{eV}$ for $t' \leq 0.5t$ to $W = 0.36\text{ eV}$ for $t' = t$ with $|t| = 0.04\text{ eV}$ and $T = 38.4\text{ K}$.

double occupancy with U for different t'/t and a triangular lattice. The critical values of U , U_{c1} and U_{c2} , increase with t'/t but the general behavior is similar up to $t'/t = 0.5$. At $t' \sim 0.6t$ there is a more rapid change in the absolute value of the double occupancy and its dependence on U . Such behavior is roughly correlated with a crossing in the cluster energy level structure discussed above (see Fig. 7). As we will discuss below this change from non-degenerate to nearly degenerate cluster energy levels can lead to a qualitative change in the spectral properties of the cluster when coupled to the bath. As shown in the right part of the figure, the dependence of U_{c2} with t'/t follows the dependence of the bandwidth W on t'/t only for $t'/t > 0.5$. Below $t'/t < 0.5$, U_{c2} increases with t'/t despite the fact that the bandwidth remains constant at the value for the square lattice: $W = 8|t| = 0.32\text{ eV}$.

D. Phase diagram

In Fig. 10 we present a phase diagram of the Hubbard model for $t' = 0$ and $t' = 0.4t$ obtained from DCA on $N_c = 8$ clusters. Based on the behavior of the double occupancy, discussed above, we have determined the critical values of U , $U_{c1}(T)$ and $U_{c2}(T)$. Between these two values there is a coexistence region, where both a metallic and an insulating phase can exist. The phase diagram also shows the pseudogap phase which occurs below the temperature, T_{PG} . This is determined by from the spectral function $A(\mathbf{K}, \omega)$ at $\mathbf{K} = (\pi, 0)$. A suppression of the weight at $\omega = 0$ marks the onset of the pseudogap phase. A crossover region above the coexistence region is determined from the spectra. In this region there is no proper quasiparticle at the chemical potential but also no proper Mott gap. The quantity T_{spin} is obtained for a fixed U as the T where $\langle S_i^z S_j^z \rangle = -0.15$ for i and j nearest neighbor. In Fig. 11, showing results for a frustrated model, the criteria was set to -0.20 . In a similar way

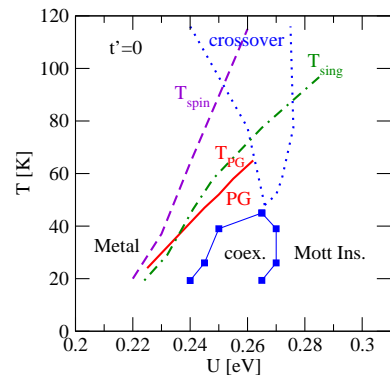


FIG. 10. (Color online) Temperature vs. U phase diagram for the half-filled Hubbard model from self-consistent DCA for the unfrustrated system ($t' = 0$). Metallic, Mott insulating and crossover regions are shown. The temperature scales T_{spin} and T_{sing} denote temperatures below which spin and d -wave pairing correlations, respectively, become substantial. T_{PG} indicates the temperature scale below which a pseudogap opens up in the $(\pi, 0)$ spectral density. The parameters are $t = -0.04\text{ eV}$ and $N_c = 8$.

we have determined T_{sing} as the T where $P_{x^2-y^2} = 0.19$, slightly more than half the maximum value in Fig. 3 of the pairing correlation.

The phase diagram displays metallic, Mott insulating, 'coexistence' and pseudogap phases. The crossover region which separates the Mott insulating and metallic phases is shown. The phase diagram with $t' = 0.4t$ should be compared to the phase diagram⁴³ of the organic salt κ -(BEDT-TTF)₂Cu[N(CN)]₂Cl.

The $U_c(T)$ boundaries shown in Fig. 10 display a positive slope in contrast to single site DMFT. This difference is attributed to short range non-local correlations which occur at sufficiently low temperatures and are neglected in DMFT.^{36,48} Such behavior was also found previously on $N_c = 4$ clusters.^{36,48} Magnetic correlations lead to a suppression of entropy at low T , $S \rightarrow 0$ as $T \rightarrow 0$. With increasing T , the system gains entropy by transforming into a metallic state since $S \propto T$ in the metal.⁴⁰ At higher temperatures the system can gain further entropy by transforming back into the paramagnetic insulating state with entropy $S \sim \ln(2)$. Hence, a reentrant behavior of the phase diagram occurs. The phase diagram resembles the experimental phase diagram with small degree of geometrical frustration of the organic salts, such as κ -(BEDT-TTF)₂Cu[N(CN)]₂Cl.⁴⁹ In particular, the positive slope of the $U_{c1}(T)$ and $U_{c2}(T)$ boundaries and the reentrant behavior agree with experiment.

E. Effective mass enhancement and non-Fermi liquid behavior

We introduce the quasiparticle weight $Z_{\mathbf{k}} = 1/(1 - d\Sigma(\mathbf{k}, \omega)/d\omega)$ and approximate $d\Sigma(\mathbf{k}, \omega)/d\omega \approx \Sigma(\mathbf{k}, i\omega_0)/(i\omega_0)$, where $\omega_0 = \pi/\beta$ with $\beta = 300\text{ eV}^{-1}$

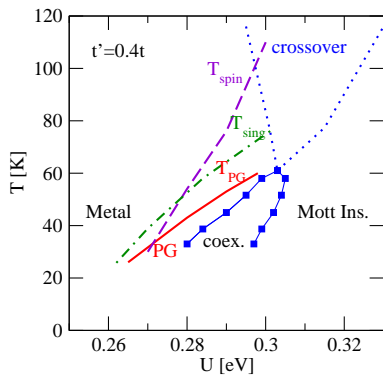


FIG. 11. (Color online) The same as in Fig. 10, but for the frustrated anisotropic triangular lattice with $t' = 0.4t$.

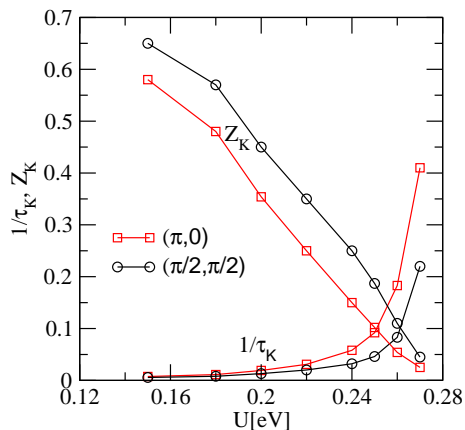


FIG. 12. (Color online) Quasiparticle effective mass and scattering rate dependence with U from self-consistent DCA. The parameters are $t = -0.04$ eV, $t' = 0$ and $T = 38.4$ K.

($T = 38.4$ K). We also introduce the scattering rates, $1/\tau_{\mathbf{k}} = -\text{Im} \Sigma(\mathbf{k}, i\omega_0)$. In Fig. 12 we show the dependence on U of $Z_{\mathbf{K}}$ and $1/\tau_{\mathbf{K}}$ at the patch momenta \mathbf{K} . $Z_{\mathbf{K}}$ is gradually suppressed with U . At about $U \approx 0.22 - 0.24$ eV and $t' = 0$ the $\mathbf{K} = (\pi, 0)$ and $(\pi/2, \pi/2)$ sectors display an enhancement of $1/\tau_{\mathbf{K}}$ suggesting a non vanishing scattering rate at the Fermi surface signaling non-Fermi liquid behavior.^{19,22–24,66} At this point $Z_{\mathbf{k}}$ loses the meaning of a quasiparticle weight. A momentum differentiation is clearly seen in $1/\tau_{\mathbf{K}}$ between $\mathbf{K} = (\pi/2, \pi/2)$ and $\mathbf{K} = (\pi, 0)$. This differentiation grows as the Mott metal-insulator transition is approached.

It is useful to explore further the non-Fermi liquid behavior found at different \mathbf{K} -points on the Fermi surface by analyzing the self-energy in real space. In Fig. 13 we show the real space self-energy, $\Sigma_{c,ij}(i\omega_n)$. The imaginary part of the on-site self-energy of the cluster, $\text{Im} \Sigma_{c,ii}(i\omega_n)$, shows non-Fermi liquid behavior since it goes to a finite value as $\omega_n \rightarrow 0$. In addition, the imaginary part of the off-diagonal self-energy between next-nearest neighbor sites, $\text{Im} \Sigma_{c,\langle\langle ij \rangle\rangle}(i\omega_n)$, shows a significant enhancement in the pseudogap phase close to the

Mott transition.

Expressing $\Sigma_c(\mathbf{K}, i\omega_n)$ in terms of its real space components $\Sigma_{c,ij}(i\omega_0)$ through the Fourier transform¹⁹

$$\Sigma_c(\mathbf{K}, i\omega) = \frac{1}{N_c} \sum_{i,j} e^{i\mathbf{K}\cdot(\mathbf{R}_i - \mathbf{R}_j)} \Sigma_{c,ij}(i\omega), \quad (17)$$

we find that the self-energy in momentum space can be approximated by:

$$\begin{aligned} \Sigma_c((\pi, 0), i\omega) &\approx \Sigma_{c,ii}(i\omega) - 2\Sigma_{c,\langle\langle ij \rangle\rangle}(i\omega) \\ \Sigma_c((\pi/2, \pi/2), i\omega) &\approx \Sigma_{c,ii}(i\omega), \end{aligned} \quad (18)$$

since the real space contributions from the more distant neighbors is negligible. Therefore, $\Sigma_c((\pi/2, \pi/2), i\omega)$ basically coincides with the on-site self-energy. The $(\pi, 0)$ self-energy is enhanced with respect to $\Sigma_c((\pi/2, \pi/2), i\omega)$ because of the additional off-diagonal contribution $\Sigma_{c,\langle\langle ij \rangle\rangle}(i\omega_n)$ not present at $(\pi/2, \pi/2)$ due to the phase factors. The momentum differentiation can then be related to the enhancement of the off-diagonal next-nearest neighbors self-energy, $\Sigma_{c,\langle\langle ij \rangle\rangle}(i\omega_n)$.¹⁹ Such enhancement is also encountered in smaller $N_c = 4$ clusters, but is missed by single-site DMFT calculations which neglect the spatial dependence of the self-energy. Earlier CDMFT calculations on $N_c = 4$ clusters find similar enhancement,¹⁹ although in such small clusters interpolation schemes are need to compute the self-energy at $(\pi/2, \pi/2)$. Also in the $N_c = 3$ clusters a similar behavior of the off-diagonal self-energy with U arises close to the Mott transition. Even a cluster with $N_c = 2$ gives momentum differentiation if the patches are chosen appropriately.²² In conclusion, non-Fermi liquid behavior is found in the on-site self-energies of the cluster embedded in the metallic host. The next-nearest neighbors self-energy are directly responsible for the momentum differentiation.

F. Importance of internal structure of cluster: first iteration DCA.

Fig. 14 compares DCA calculations where the bath is determined self-consistently with DCA calculations where the bath is determined from the noninteracting Hamiltonian, i.e., using Eqs. (4, 6) with $\Sigma_c \equiv 0$. We refer to this as the first iteration. The figure illustrates that a pseudogap is obtained also in the first iteration, although for a larger U than in the self-consistent calculation. In the self-consistent case the bath can form a pseudogap itself and it is then difficult to separate how much the pseudogap in the spectral function is a result of these modifications of the bath and how much is due to other factors. In the first iteration the bath is fully metallic and the pseudogap formation is entirely due to the internal structure of the cluster and to different couplings to the bath for different \mathbf{k} -vectors which also exist in the first iteration. As the results are iterated any tendency to pseudogap formation is enhanced by similar

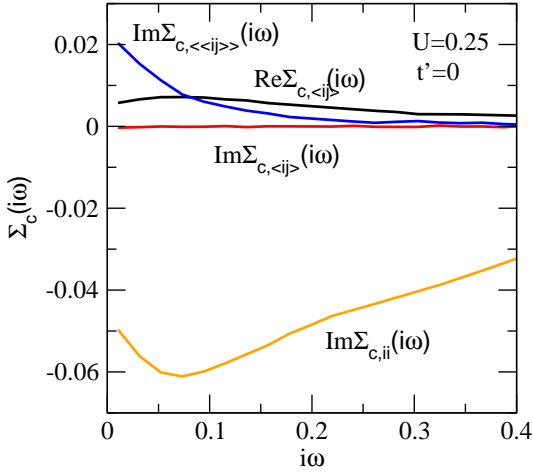


FIG. 13. (Color online) Cluster self-energy components in real space obtained from Fourier transforming the self-consistent DCA self-energy in a $N_c = 8$ cluster for $t = 0.04$ eV and at $T = 38.4$ K. The on-site (Σ_{ii}), nearest neighbor ($\Sigma_{(ij)}$) and next-nearest neighbor ($\Sigma_{\langle\langle ij \rangle\rangle}$) self-energies are shown. The imaginary part of the next-nearest neighbor self-energy is enhanced as the Mott transition is approached leading to differences in the $(\pi/2, \pi/2)$ and $(\pi, 0)$ sectors at the Fermi surface.

modifications in the bath. This approach makes it easier to identify the driving force for pseudogap formation.

It is interesting to compare with dynamical mean-field theory (DMFT), i.e., $N_c = 1$. The self-consistent calculation describes the formation of a Mott insulator for appropriate parameters, while the first iteration always gives a Kondo peak (although possibly with very little weight) for a metallic bath. The occurrence of a pseudogap already in the first iteration in DCA shows that the internal structure of the cluster is important for the formation of the pseudogap.

In the Coulomb interaction a parameter n_0 is introduced [Eq. (2)]. This has the effect of transferring weight from the self-energy to the one-particle part of the Hamiltonian. This plays a particular role when the calculation is stopped after the first iteration and the self-energy is neglected in generating the bath. As a measure of the importance of the self-energy we use

$$\sum_{i=1}^{N_c} \sum_{0 < \omega_n < \omega_{\max}} |\Sigma_c(\mathbf{K}_i, \omega_n)|^2. \quad (19)$$

This quantity is shown in Fig. 15. As discussed below Eq. (2), the choice $n_0 = n/2$ leads to $\Sigma_c(\mathbf{K}_i, \omega_n) \rightarrow 0$ for $\omega_n \rightarrow \infty$. This is illustrated by the flatness of the curve for $n_0 = 0.46 = (n/2)$ for large ω_{\max} . But this choice also reduces $\Sigma_c(\mathbf{K}_i, \omega_n)$ substantially for small values of ω_n . Therefore, $n_0 = n/2$ is the optimum choice of n_0 in the first iteration calculation, where $\Sigma_c(\mathbf{K}_i, \omega_n)$ is neglected when calculating the bath.

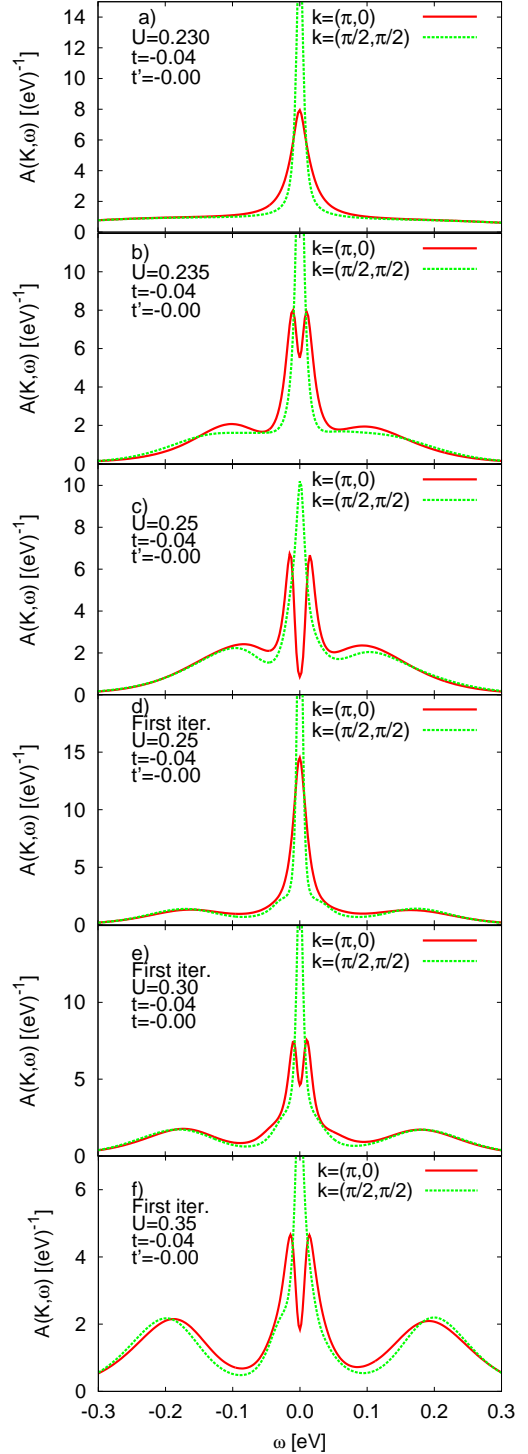


FIG. 14. Spectral functions $A(\mathbf{k}, \omega)$ for $\mathbf{k} = (\pi, 0)$ and $(\pi/2, \pi/2)$. The parameters are $t = -0.04$ eV, $t' = 0$, $N_c = 8$ and $T = 38$ K. Figs. a-c) show self-consistent results, while d-f) show results after one iteration. The figures illustrate how in both cases a pseudogap opens for $\mathbf{k} = (\pi, 0)$, although for smaller values of U for the self-consistent case.

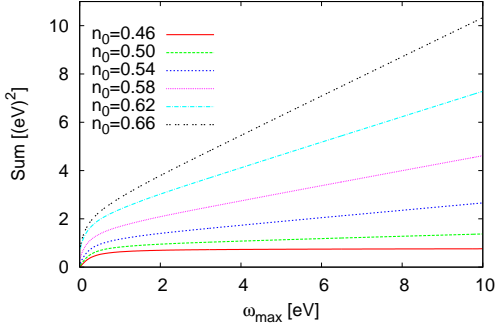


FIG. 15. Sum over the absolute value of the self-energy squared. The parameters are $t = -0.04$ eV, $t' = 0.012$ eV, $N_c = 8$, $U = 0.3$ eV and $T = 58$ K. The filling is $n = 0.92$. The figure illustrates that the optimum $n_0 = n/2 = 0.46$.

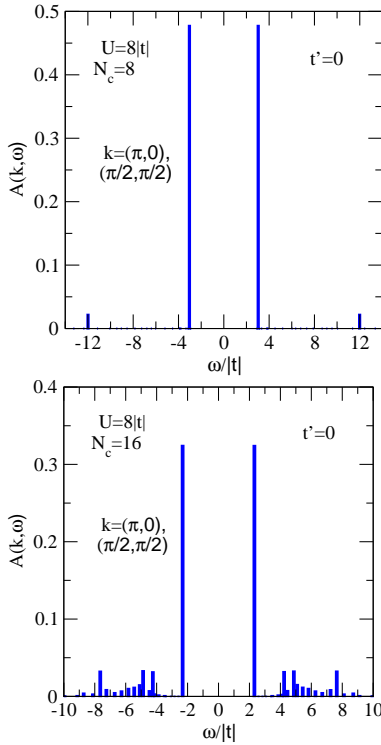


FIG. 16. Spectral function for isolated $N_c = 8$ and $N_c = 16$ clusters. The figure illustrates that the $\mathbf{k} = (\pi, 0)$ and $\mathbf{k} = (\pi/2, \pi/2)$ spectra are identical. The parameters are $U = 8|t_{\text{cluster}}|$ and $t' = 0$.

G. Importance of coupling to bath

One might expect to see signs of a pseudogap already for an isolated cluster, calculating the spectrum using exact diagonalization (ED). A finite cluster only has discrete peaks and we expect a gap. However, one might expect that either the gap would be smaller for $\mathbf{k} = (\pi/2, \pi/2)$ or that weight of the lowest binding energy peak would be larger for $\mathbf{k} = (\pi/2, \pi/2)$ than

$\mathbf{k} = (\pi, 0)$. However, Fig. 16 shows that the two spectra are identical for $N_c = 8$ (cluster 8A) and $N_c = 16$ (cluster 16B), contradicting this expectation. Actually, it has been shown⁶⁷ that there is an additional symmetry for these two clusters, which make the two spectra identical.

The pseudogap is, however, clearly observed in DCA calculations with $N_c = 8$. The pseudogap must then also be related to the coupling to the bath. To test this we have performed DCA calculations where the couplings to the bath for the nodal and anti-nodal points have been switched. The results are shown in Fig. 17. Indeed, the pseudogap then appears at $\mathbf{k} = (\pi/2, \pi/2)$. As discussed in Sec. II the coupling to the bath is stronger for $\mathbf{k} = (\pi/2, \pi/2)$. Switching the coupling then leads to a weaker coupling for this \mathbf{k} -point and it also leads to a pseudogap.

The numerical experiment in Sec. III F, performing only one iteration, demonstrated the importance of the internal structure of the cluster. The additional experiment in Fig. 17 demonstrates that the coupling to the bath also plays a crucial role.

For sufficiently large, $U \gg t$, the excitation spectra of the cluster shows that the charge gap: $\Delta_g = E_0(N+1) + E_0(N-1) - 2E_0(N)$ differs from the gap that is extracted from photoemission. For instance, for $U = 30t$ and $N = 8$ we find: $\Delta_g = 24.5932|t|$, whereas the gap extracted from the lowest energy peaks in $A(\mathbf{k}, \omega)$ is $26.588|t|$. The difference between the two gaps comes from the fact that the lowest state with one hole is the Nagaoka state with a total spin $S = (N-1)/2$ for $U \gg t$ which is $1.002t$ below the $S = 1/2$ state. Since the total spin should be conserved in the photoemission process, the $S = (N-1)/2$ state has zero matrix element:

$$\langle \Psi_0(N-1) | c_{k\sigma} | \Psi_0(N) \rangle = 0, \quad (20)$$

and is not observed in photoemission while the $S = 1/2$ state above it would have a non-zero photoemission matrix element since it conserves the total spin of the system.

H. Formulation in k-space

The behavior of the spectral functions and pseudogap can be analyzed in a more transparent way using a momentum representation of the Hubbard model which we introduce here.

The Coulomb part of the Hamiltonian is

$$H_U = \frac{1}{2} \sum_{\mathbf{k}_1, \mathbf{k}_2, \mathbf{k}_3, \mathbf{k}_4, \sigma, \sigma'} F_{\mathbf{k}_1 \mathbf{k}_2 \mathbf{k}_3 \mathbf{k}_4} c_{\mathbf{k}_1 \sigma}^\dagger c_{\mathbf{k}_2 \sigma'}^\dagger c_{\mathbf{k}_4 \sigma'} c_{\mathbf{k}_3 \sigma}. \quad (21)$$

Since the Coulomb interaction is on-site, the Coulomb integral F takes the form

$$\begin{aligned} F_{\mathbf{k}_1 \mathbf{k}_2 \mathbf{k}_3 \mathbf{k}_4} &= \frac{U}{N^2} \sum_{l=1}^N e^{-i(\mathbf{k}_1 + \mathbf{k}_2 - \mathbf{k}_3 - \mathbf{k}_4) \cdot \mathbf{R}_l} \\ &= \frac{U}{N} \delta_{\mathbf{k}_1 + \mathbf{k}_2 - \mathbf{k}_3 - \mathbf{k}_4}. \end{aligned} \quad (22)$$

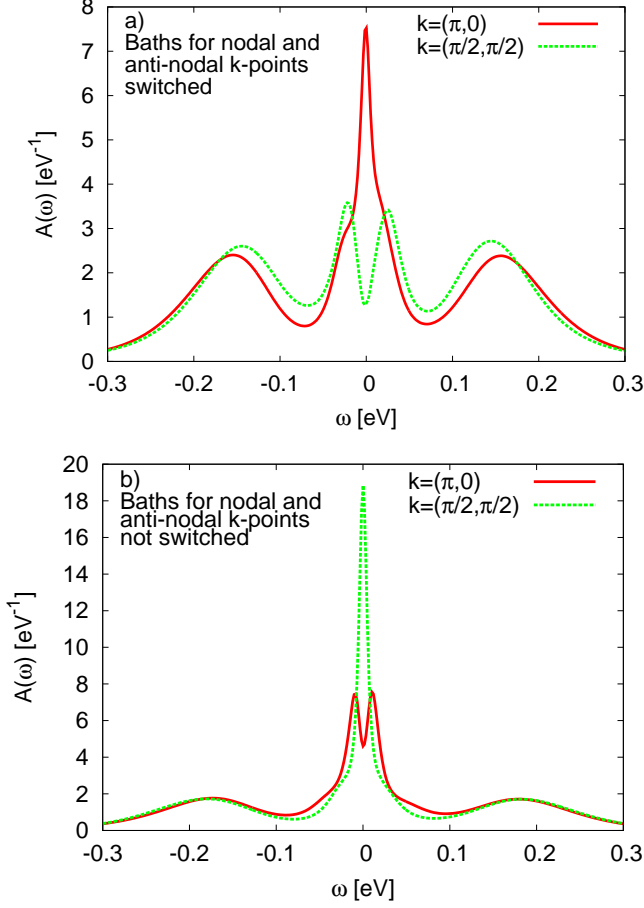


FIG. 17. Spectral function for $N_c = 8$. In a) the baths for the nodal and anti-nodal points have been switched, while in b) this is not the case. The figure illustrates that switching the baths (a) leads to a pseudogap for $\mathbf{k} = (\pi/2, \pi/2)$ instead of $\mathbf{k} = (\pi, 0)$ as in b). The parameters are $U=0.3$ eV, $t=-0.04$ eV, $t' = 0$ and $T = 38.4$ K. The results were obtained in the first iteration.

We can then write the Hamiltonian as

$$H_U = \frac{U}{N} \sum_{\mathbf{k}} n_{\mathbf{k}\uparrow} n_{\mathbf{k}\downarrow} + \frac{1}{2} \frac{U}{N} \sum_{\mathbf{k} \neq \mathbf{k}' \sigma \sigma'} n_{\mathbf{k}\sigma} n_{\mathbf{k}'\sigma} + \frac{U}{N} \sum_{\mathbf{k}, \mathbf{k}', \mathbf{q} \neq 0, \sigma \sigma'} c_{\mathbf{k}\sigma}^\dagger c_{\mathbf{k}'\sigma'}^\dagger c_{\mathbf{k}'-\mathbf{q}\sigma'} c_{\mathbf{k}+\mathbf{q}\sigma}$$

The total Hamiltonian is then

$$H = H_U + \sum_{\mathbf{k}\sigma} \varepsilon_{\mathbf{k}} n_{\mathbf{k}\sigma}, \quad (23)$$

where $\varepsilon_{\mathbf{k}}$ depends on the model used.

It is interesting to study the lowest states for an isolated cluster with $N_c = 4$. We label the \mathbf{k} -vectors as $\mathbf{k}_1 = (0, 0)$, $\mathbf{k}_2 = (\pi, 0)$, $\mathbf{k}_3 = (0, \pi)$ and $\mathbf{k}_4 = (\pi, \pi)$. Then the dominating configurations in the three lowest

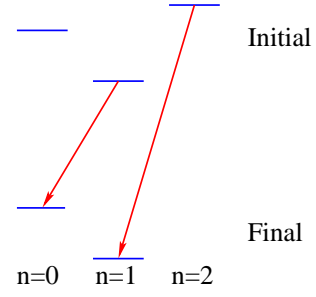


FIG. 18. Schematic level diagram for the model in Eq. (26) in the absence of bath-cluster hopping. The number of electrons on the c site is given by n . The arrows show which configurations are connected in the photoemission process. An electron is removed from site c , and the initial configurations with $n = 1$ and 2 are connected to final configurations with $n = 0$ or 1 , respectively.

states are

$$\begin{aligned} |1\rangle &= a_1(|21, 21\rangle - |31, 31\rangle) \\ |2\rangle &= a_2(|21, 31\rangle - |31, 21\rangle) \\ |3\rangle &= a_3(|21, 21\rangle + |31, 31\rangle). \end{aligned} \quad (24)$$

Here the first two numbers in each ket gives the two spin up electrons and the following two numbers the spin down electrons. For $|U/t| = 5$ the coefficients are $a_1 = 0.64$, $a_2 = 0.61$ and $a_3 = 0.47$. The terms in Eq. (24) then represent 81, 74 and 45 per cent of the total weight.

For $N_c = 8$ we also include the four \mathbf{k} -vectors $\mathbf{k}_5 = (\pi/2, \pi/2)$, $\mathbf{k}_6 = (-\pi/2, \pi/2)$, $\mathbf{k}_7 = (\pi/2, -\pi/2)$ and $\mathbf{k}_8 = (-\pi/2, -\pi/2)$. The dominating terms in the lowest state of the isolated cluster is then

$$\begin{aligned} |1\rangle &= a(-|1368, 1368\rangle + |1378, 1378\rangle + |1356, 1356\rangle \\ &\quad - |1357, 1357\rangle - |1278, 1278\rangle + |1268, 1268\rangle \\ &\quad + |1257, 1257\rangle - |1256, 1256\rangle), \end{aligned} \quad (25)$$

where $a = 0.24$ for $U/t = 5$. This corresponds to a total weight of about 0.44, meaning that there are many other terms which are not very much smaller. However, we notice the tendency for both $N_c = 4$ (in particular) and $N_c = 8$ to have configurations where the same \mathbf{k} -vectors are occupied both for spin up and down. This plays an important role for the following discussion.

IV. TWO-LEVEL MODEL

We first consider a very simple example, namely a two-level model. This model illustrates some important interference effects and the tendency to transfer spectral weight to the Fermi energy.^{68,69} We introduce the model

$$\begin{aligned} H_0 &= \varepsilon_b \sum_{\sigma} n_{b\sigma} + \varepsilon_c \sum_{\sigma} n_{c\sigma} \\ &\quad + \sum_{\sigma} V(c_{b\sigma}^\dagger c_{c\sigma} + c_{c\sigma}^\dagger c_{b\sigma}) + U n_{c\uparrow} n_{c\downarrow}. \end{aligned} \quad (26)$$

Here $c_{b\sigma}^\dagger$ creates an electron on site b with the spin σ , and $n_{c\sigma} = c_{c\sigma}^\dagger c_{c\sigma}$. The electron can hop between sites b and c with a hopping integral $V (< 0)$. On site c there is a on-site Hubbard Coulomb integral U . In the language of a DCA calculation, site c corresponds to a cluster site in a cluster with one atom and b corresponds to a bath with just one level. The system has two electrons in the initial state. We form three configurations,

$$\begin{aligned} |0\rangle &= c_{b\uparrow}^\dagger c_{b\downarrow}^\dagger |\text{vac}\rangle \\ |1\rangle &= (1/\sqrt{2})(c_{b\uparrow}^\dagger c_{c\downarrow}^\dagger + c_{c\uparrow}^\dagger c_{b\downarrow}^\dagger) |\text{vac}\rangle \\ |2\rangle &= c_{c\uparrow}^\dagger c_{c\downarrow}^\dagger |\text{vac}\rangle \end{aligned} \quad (27)$$

with zero, one or two electrons, respectively, on the c site. Here $|\text{vac}\rangle$ is a state with no electrons. The ground-state can then be written as

$$|\Phi\rangle = a_0|0\rangle + a_1|1\rangle + a_2|2\rangle, \quad (28)$$

where a_i are coefficients determined by the parameters. We now consider a photoemission process, where a spin down electron is removed from site c of the ground-state, leading to final states with just one electron. This is illustrated in Fig. 18. This process connects initial configurations with one or two electrons on the c site to final configurations with zero or one electron, respectively, on the c site. The corresponding final states are

$$|+\rangle = b_0|\tilde{0}\rangle + b_1|\tilde{1}\rangle, \quad |-\rangle = b_1|\tilde{0}\rangle - b_0|\tilde{1}\rangle, \quad (29)$$

where $|\tilde{0}\rangle$ and $|\tilde{1}\rangle$ have an electron on the b or c site, respectively. For $V < 0$ all coefficients are positive. The spectral weights are

$$|\langle +|c_{c\downarrow}|\Phi\rangle|^2 = \left| \frac{b_0 a_1}{\sqrt{2}} + b_1 a_2 \right|^2, \quad |\langle -|c_{c\downarrow}|\Phi\rangle|^2 = \left| \frac{b_1 a_1}{\sqrt{2}} - b_0 a_2 \right|^2 \quad (30)$$

Here $|\langle +|c_{c\downarrow}|\Phi\rangle|^2$ is the weight of the leading peak with low binding energy and $|\langle -|c_{c\downarrow}|\Phi\rangle|^2$ the weight of a satellite with large binding energy. The corresponding structures in an Anderson impurity model are the Kondo peak and the Hubbard side band, respectively. For $U \gg |t|$ and $\varepsilon_c \approx -U/2$, a_1 and b_1 are large and all other coefficients are small. We might then expect most of the weight in the Hubbard side band. However, there is constructive interference for the low binding energy peak and destructive interference for the high energy peak. The result is a transfer of weight towards the Fermi energy.^{68,69}

This just reflects that the lowest initial and final states are both bonding. This effect is important. To illustrate this let us consider the case when there is now hopping in the final state. Then $b_1 = 1$ and $b_0 = 0$, and the peaks in the spectrum gives direct information about the weights a_1^2 and a_2^2 of the initial configurations $|1\rangle$ and $|2\rangle$, respectively. For instance, we use $\varepsilon_b = 0$, $\varepsilon_c = -2$, $V = -1$ and $U = 4$. With $b_1 = 1$ and $b_0 = 0$, we would then find the weights of the low and high energy peaks to be 0.14 and 0.36, respectively. This simply reflects that the parameters are such that the $n = 1$ configuration has most

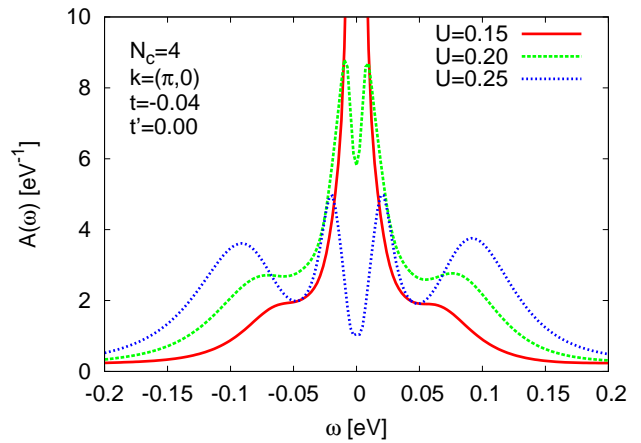


FIG. 19. Spectral function for a DCA calculation with a four site cluster as a function of U . The parameters are $t = -0.04$ eV, $t' = 0$ and $T = 29$ K. The results were obtained after the first iteration.

of the weight (0.72) in the initial state. This couples to the final configuration $n = 0$, which corresponds to the excited state. Properly taking into account interference, on the other hand, reverses the weights and leads to the weights 0.33 and 0.17 for the low and high binding energy peaks, respectively. These effects are crucial for building up spectral weight in the neighborhood of the Fermi energy. However, the model considered in Eq. (26) cannot explain a pseudogap. To do this we need to generalize to a four-level model, where the cluster (here site c) has an internal structure. This is done in the next section.

V. FOUR-LEVEL MODEL

A DCA calculation for $N_c = 4$ shows a pseudogap, even in the first iteration, as is shown in Fig. 19. We can therefore use such a cluster to study the origin of the pseudogap. Actually, we can make even more simplifications. The four site cluster has only four wave vectors \mathbf{K} . Two of these, $\mathbf{K} = (0, 0)$ and $\mathbf{K} = (\pi, \pi)$, have one-particle energies which are fairly far from the Fermi energy at half-filling. We then expect the main physics to be determined by $\mathbf{K}_1 = (\pi, 0)$ and $\mathbf{K}_2 = (0, \pi)$. For simplicity we then study a model with a cluster with just these two levels.

An alternative two-level cluster model was studied by Ferrero *et al.*²² They introduced a two patch model in momentum space, which simulates the $(\pi, 0)$ and $(\pi/2, \pi/2)$ points on the Fermi surface. This model allows a study of the important \mathbf{k} -dependence of the pseudogap, and it was interpreted in terms of an orbital selective Mott transition.^{70,71} However, such a model oversimplifies the real situation in the interesting intermediate U -regime where the pseudogap opens up in the $(\pi, 0)$, $(0, \pi)$ but not in the $(\pm\pi/2, \pm\pi/2)$ sector. We find below that for such values of U there is a strong correlation between

the $(\pi, 0)$ and $(0, \pi)$ levels, which is important for the opening of the pseudogap. This effect is not available in Ref. 22 when there is a pseudogap for $(\pi, 0)$ but a peak for $(\pi/2, \pi/2)$, since the $(\pi/2, \pi/2)$ level then primarily couples to its bath and not to $(\pi, 0)$. This effect is included in the four-level model below at the price of not being able to describe the important \mathbf{k} -dependence. For this purpose we later study a $N_c = 8$ model, which has the proper \mathbf{k} -dependence, and show that the essential parts of the physics in the four-level model survive in the $N_c = 8$ calculation.

The cluster \mathbf{k} -states are each connected to their own baths. For simplicity, we assume that each bath has just one level. This leads to a four-level model with two two-fold degenerate orbitals. This model shows some important effects related to the pseudogap and is relatively easy to analyze. The one-particle part is given by

$$H_0 = \varepsilon_c \sum_{i=1}^2 \sum_{\sigma} n_{ic\sigma} + \varepsilon_b \sum_{i=1}^2 \sum_{\sigma} n_{ib\sigma} + V \sum_{i\sigma} (\psi_{ic\sigma}^\dagger \psi_{ib\sigma} + \psi_{ib\sigma}^\dagger \psi_{ic\sigma}). \quad (31)$$

where c refers to cluster levels and b to bath levels. We add a Coulomb interaction with multiplet effects on the c site

$$H_U = U_{xx} \sum_{i=1}^2 n_{ic\uparrow} n_{ic\downarrow} + U_{xy} \sum_{\sigma\sigma'} n_{1c\sigma} n_{2c\sigma'} + K (\psi_{1c\uparrow}^\dagger \psi_{1c\downarrow}^\dagger \psi_{2c\downarrow} \psi_{2c\uparrow} + h.c.) - K \sum_{\sigma} \psi_{1c\sigma}^\dagger \psi_{2c\sigma}^\dagger \psi_{2c\sigma} \psi_{1c\sigma} - K \sum_{\sigma} \psi_{1c-\sigma}^\dagger \psi_{2c\sigma}^\dagger \psi_{2c-\sigma} \psi_{1c\sigma}. \quad (32)$$

The fourth term is a diagonal term favoring parallel spins, i.e., a Hund's rule coupling. The interaction term, H_U , can be expressed in the standard Kanamori form used in the context of multiorbital band models by taking: $U_{xx} = U$ and $U_{xy} = U - 2K$. Here we take a different approach. As discussed in Appendix X, the level structure of the four-site cluster can be simulated by using $U_{xx} < U_{xy}$. The lowest state of the isolated site c is then a singlet. Alternatively, we can use $U_{xx} > U_{xy}$, which leads to a triplet ground-state for site c . As we will see, the physics is quite different in the two cases. We write $U_{xx} = U - \Delta U$ and $U_{xy} = U + \Delta U$, using $\Delta U = 0.03U$, $K = 0.1U$ and $V = -0.02$ eV. We consider the symmetric case where $\varepsilon_b = 0$ and $\varepsilon_c = -3U/2 + (K - \Delta U)/2$. This model is shown schematically in Fig. 20.

The interaction part H_U of our four-level model differs from the two-orbital Anderson model introduced⁵⁰ in the context of A_3C_{60} since pair-hopping terms are not present in that model so that spin rotational symmetry is broken. We note that the pair-hopping term is important for inducing a ground state of the type in Eq. (24) and (25) containing doubly-occupied sectors. Previous studies in the context of multiband models for transition metal oxides and fullerenes focus on the effect

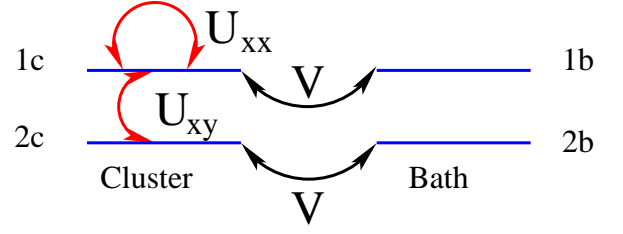


FIG. 20. Schematic picture of the four-level model.

of ferromagnetic Hund's coupling-type exchange between electrons on different orbitals with the same^{50,72,73} or different bandwidths^{70,74} on the Mott transition. We note that the Hubbard model leads to particular Coulomb interaction terms which in general differ from multiband models.

We first study the isolated c site, which has the $S_z = 0$ two-electron configurations

$$\begin{aligned} |a\rangle &= c_{1c\uparrow}^\dagger c_{1c\downarrow}^\dagger |\text{vac}\rangle \\ |b\rangle &= c_{2c\uparrow}^\dagger c_{2c\downarrow}^\dagger |\text{vac}\rangle \\ |c\rangle &= c_{1c\uparrow}^\dagger c_{2c\downarrow}^\dagger |\text{vac}\rangle \\ |d\rangle &= c_{2c\uparrow}^\dagger c_{1c\downarrow}^\dagger |\text{vac}\rangle \end{aligned} \quad (33)$$

and the eigenenergies and states

$$\begin{aligned} E_{1-} &= U_{xx} - K; & |1-\rangle &= \frac{1}{\sqrt{2}}(|a\rangle - |b\rangle) \\ E_{2-} &= U_{xy} - K; & |2-\rangle &= \frac{1}{\sqrt{2}}(|c\rangle - |d\rangle) \\ E_{1+} &= U_{xx} + K; & |1+\rangle &= \frac{1}{\sqrt{2}}(|a\rangle + |b\rangle) \\ E_{2+} &= U_{xy} + K; & |2+\rangle &= \frac{1}{\sqrt{2}}(|c\rangle + |d\rangle) \end{aligned} \quad (34)$$

$|2-\rangle$ is a triplet, while the other states are singlets. We can also form triplet states with $S_z = \pm 1$.

For the sake of comparison, we note that our highest non-degenerate singlet state, $|2+\rangle$, is equivalent to the lowest eigenstate of the two-orbital model⁵⁰ when the exchange coupling, $K < 0$, and the degenerate triplet $|2-\rangle$ to the lowest eigenstate when $K > 0$.

To study the nature of the ground-state, we calculate the correlation functions $C_{i\sigma j\sigma'}$ between occupation numbers defined in Eq. (14) and the spin correlation function

$$S_{1c1b} = \langle \Phi | \mathbf{S}_{1c} \cdot \mathbf{S}_{1b} | \Phi \rangle, \quad (35)$$

where $|\Phi\rangle$ is the ground-state and \mathbf{S}_{1x} is the spin operator of level 1 on the site x . S_{1c1b} measures the spin correlation between level 1c and 1b. This term is expected to be important if the system is in a Kondo like state. We also calculate the kinetic (hopping) energy T_K and the "off-diagonal" Coulomb energy E_K , due to terms connecting configurations with different occupation numbers on the site c . Finally, we calculate the weights w_1 and w_2 in the

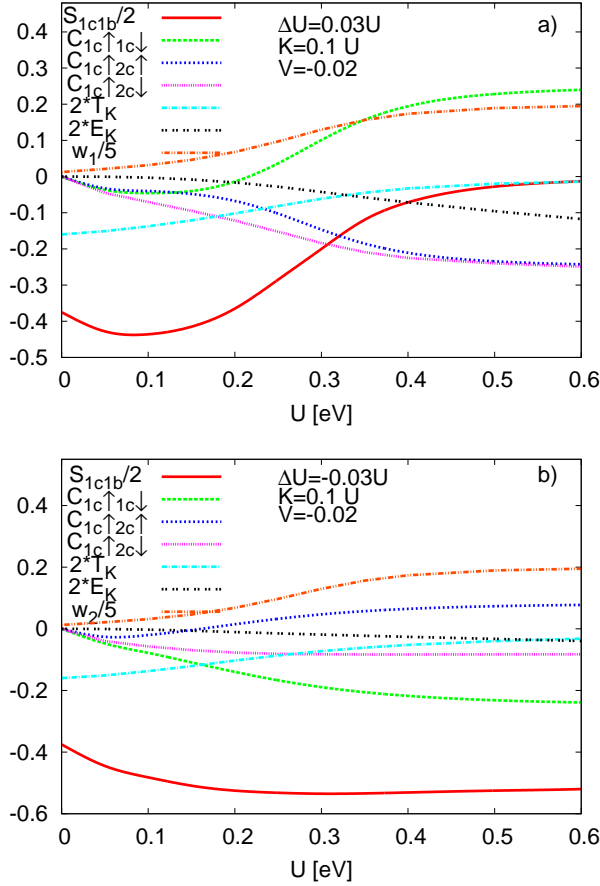


FIG. 21. Correlation functions $C_{1\uparrow 1\downarrow}$, $C_{1\uparrow 2\uparrow}$, $C_{1\uparrow 2\downarrow}$, S_{1c1b} [Eq. (35)], hopping energy T_K , "off-diagonal" Coulomb energy E_K and weight (w_1 or w_2) of the lowest c state. In a) $\Delta U = 0.03U$ and in b) $\Delta U = -0.03U$. In a) the lowest c state is a singlet and in b) a triplet. The parameters are $K = 0.1U$ and $V = -0.02$ eV.

ground-state of the c states $|1-\rangle$ and $|2-\rangle$, respectively. For $\Delta U > 0 (< 0)$ we expect w_1 (w_2) to approach unity for $U \rightarrow \infty$, since hopping between the b and c sites is then completely suppressed. In Fig. 21a ($\Delta U > 0$) we show w_1 and in Fig. 21b ($\Delta U < 0$) w_2 . Observe that both quantities have been divided by a factor of five.

We first consider $\Delta U > 0$ in Fig. 21a. For U not too large, $|T_K|$ and $|S_{1c1b}|$ are large, implying that spin correlation and coupling between the sites are important. The correlation function $C_{1c\uparrow 1c\downarrow}$ is somewhat negative

In the limit of very large U and for $\Delta U > 0$, the ground-state takes the form

$$|\Phi\rangle = \frac{1}{2}(c_{1c\uparrow}^\dagger c_{1c\downarrow}^\dagger - c_{2c\uparrow}^\dagger c_{2c\downarrow}^\dagger)(c_{1b\uparrow}^\dagger c_{1b\downarrow}^\dagger - c_{2b\uparrow}^\dagger c_{2b\downarrow}^\dagger)|\text{vac}\rangle. \quad (36)$$

The c part of the wave function then has singlet charac-

ter. If instead $\Delta U < 0$ and U is very large, we obtain

$$|\Phi\rangle = \frac{1}{\sqrt{3}}[c_{1c\uparrow}^\dagger c_{2c\uparrow}^\dagger c_{1b\downarrow}^\dagger c_{2b\downarrow}^\dagger - \frac{1}{2}(c_{1c\uparrow}^\dagger c_{2c\downarrow}^\dagger + c_{1c\downarrow}^\dagger c_{2c\uparrow}^\dagger) \times (c_{1b\uparrow}^\dagger c_{2b\downarrow}^\dagger + c_{1b\downarrow}^\dagger c_{2b\uparrow}^\dagger) + c_{1c\downarrow}^\dagger c_{2c\downarrow}^\dagger c_{1b\uparrow}^\dagger c_{2b\uparrow}^\dagger]|\text{vac}\rangle. \quad (37)$$

Here the c part has triplet character. These results confirm the discussion above.

TABLE VIII. Weights of the different states of the c cluster (Eq. 34) in the ground state of the four-level model, overlap (“over”) to the noninteracting state, results for the different terms entering Eq. (45) and weights of the low-binding energy peaks in photoemission. The estimated peak weights are obtained through the approximate expression Eq. (45) which are compared with the exact calculated weights. A near cancellation between Terms 1 and 2 leads to the vanishingly small calculated photoemission weight of Peak 1 associated with the pseudogap. The parameters are $V = -0.02$ eV, $\Delta U = \pm 0.03U$, $K = 0.1U$, $U_{xx} = U - \Delta U$ and $U_{xy} = U + \Delta U$.

U	ΔU	States				Over.	Term 1	Term 2	Term 3	Peak 1		Peak 2		Peak 3		Peak 4	
		1-⟩	Triplet	1+⟩	2+⟩					Est	Calc	Calc	Est	Calc	Calc		
2.0	.06	1.00	0.000	0.000	0.000	.42	-.00592	.00597	.00023	2.6×10^{-7}	1.3×10^{-7}	.00049	.00014	.00023	.00028		
1.0	.03	1.00	0.002	0.000	0.000	.44	-.0117	.0121	.00195	1.9×10^{-5}	0.9×10^{-5}	.0213	.00056	.00102	.00116		
0.5	.015	0.95	0.035	0.012	0.001	.57	-.0211	.0265	.0193	.0019	.0008	.012	.0023	.0057	.0055		
0.25	.0075	0.49	0.348	0.024	0.016	.89	-.0161	.0786	.141	.12	.052	.044	.0090	.029	.019		
0.10	.003	0.16	0.36	0.072	0.060	.99	-.0032	.234	.422	1.16	.31	.005	.056	.017	.007		
0.00	.000	0.06	0.19	0.063	0.063	1					.500	.000		.000	.000		
2.0	-.06	.000	1.00	.000	.000	.71	-.00206	.0105	.0087	.00066	.00065	.00052		.00076	.00095		
1.0	-.03	.002	0.99	.000	.000	.73	-.00397	.0211	.0193	.0031	.0029	.0020		.0031	.0037		
0.5	-.015	.018	0.94	.001	.003	.80	-.00682	.0432	.0516	.0195	.0151	.0072		.013	.013		
0.25	-.0075	.084	0.75	.015	.021	.91	-.00765	.0925	.152	.151	.086	.014		.075	.022		
0.1	-.008	.108	0.42	.055	.066	.99	-.00280	.248	.441	1.27	.30	.005		.023	.007		

The photoemission part of the spectral function has four peaks close to the Fermi energy and in addition peaks approximately at $U/2$ binding energy (for the symmetric case), as shown by the insets of Fig. 22. The four peaks close to $\omega = 0$ correspond to final states with a large weight of the neutral states on the c site. For $\Delta U > 0$, the peak with the second lowest binding energy corresponds to a final state which has mainly triplet character on the cluster, while for the other three low-lying peaks the character is mainly singlet. The $x^2 - y^2$ pairing correlation $P_{x^2-y^2}$ in Eq. (12) is large for the lowest neutral cluster state and zero for the others. The peaks corresponding to the exact neutral states then results from a process where a singlet $x^2 - y^2$ has been broken up. For $\Delta U < 0$, on the other hand, the lowest neutral state is a triplet.

The peaks at roughly $-U/2$ corresponding to a Hubbard band. The total weight of the photoemission spectrum is 0.5. The calculated weights of these peaks are shown in the main part of Fig. 22. For small values of U most of the weight is in the leading peak. As U is increased, the Hubbard band peak grows and the leading peak is reduced. This is along the lines discussed in Sec. IV for the two-level model. For $\Delta U > 0$, however, as U is further increased the leading peak also loses weight relative to the other peaks with small binding energy. The difference can be orders of magnitude. This corresponds to a pseudogap. For $\Delta U < 0$ and U not too large, on the other hand, the lowest binding energy peak has a larger weight than other low binding energy peaks, and there is no pseudogap. The difference between the two cases is crucial for understanding the pseudogap, and it is analyzed in the next section.

VI. INTERFERENCE

In this section we analyze why there is a pseudogap for $\Delta U > 0$ but not $\Delta U < 0$ in the four-level model. The derivation below applies to the case when there is an infinite bath and we make no particular assumptions about the cluster. We consider a case where $U \gg |V|$, where V is the hopping to the bath. The ground-state wave function can then conveniently be described in terms of configurations with an integer number of electrons on the cluster. We consider an integer average filling n_0 . We treat photoemission processes where an electron with the quantum number ν is removed from the cluster. Here ν is a combined index containing a spin index and other indices, e.g., a \mathbf{K} index. The part of the wave function corresponding to n_0 electrons can be split in two pieces

$$|\Phi_{n_0}\rangle = |0\rangle + |1\rangle, \quad (38)$$

where

$$c_\nu|0\rangle = 0 \quad \text{and} \quad c_\nu^\dagger c_\nu|1\rangle = |1\rangle. \quad (39)$$

We assume there is hopping between the bath and the cluster determined by

$$H_0 = \sum_\nu \sum_\varepsilon (V_{\nu\varepsilon} c_\nu^\dagger c_{\nu\varepsilon} + \text{h.c.}) \quad (40)$$

In the limit of very weak hopping, we approximate the part of the ground-state corresponding to $n_0 + 1$ electrons as

$$|\Phi_{n_0+1}\rangle = - \sum_{\nu'} \sum_\varepsilon \frac{V_{\nu'\varepsilon}}{\Delta E_{+ - \varepsilon}} c_{\nu'}^\dagger c_{\nu'\varepsilon} |\Phi_{n_0}\rangle, \quad (41)$$

where we have approximated the energy difference between cluster states with one extra electron (hole) and

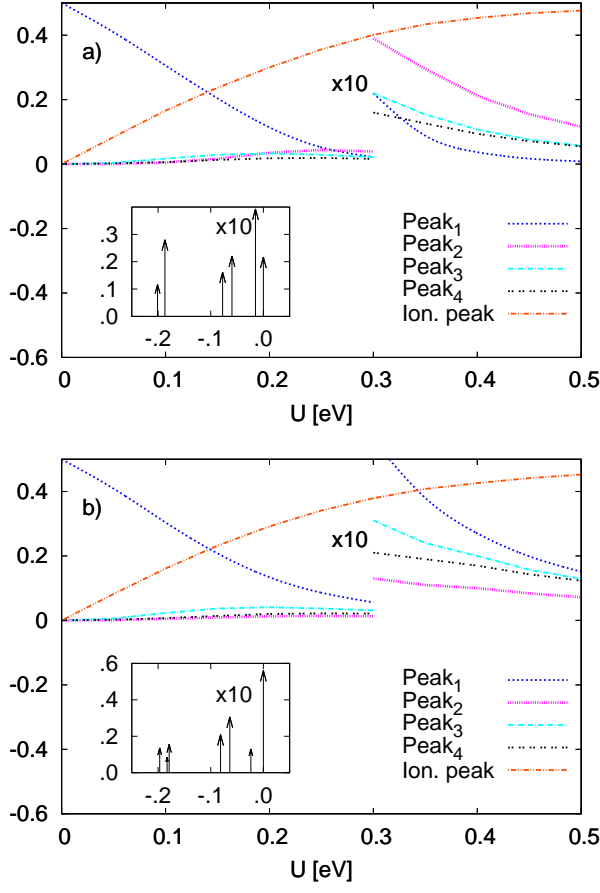


FIG. 22. Spectral weights for the four-level model. The curves show the weights of different peaks as a function of U . The inset shows the photoemission spectrum for $U = 0.3$ eV. The four low-binding energy peaks have been multiplied by a factor of 10 in the insets and main figures. In a) $\Delta U = 0.03U$ and in b) $\Delta U = -0.03U$. In a) the lowest c state is a singlet and in b) a triplet. The parameters are $K = 0.1U$ and $V = -0.02$ eV.

the lowest neutral state as ΔE_+ (ΔE_-). We write

$$|\Phi\rangle \approx |\Phi_{n_0-1}\rangle + |\Phi_{n_0}\rangle + |\Phi_{n_0+1}\rangle. \quad (42)$$

This approach looks like nondegenerate perturbation theory, and for the case of a nondegenerate ground-state of the isolated cluster this is also the case. However, in Kondo problem treated below, the states $|0\rangle$ and $|1\rangle$, which are assumed to be known, in general contain more information than can be obtained from perturbation theory, and therefore the treatment goes beyond perturbation theory. For the Kondo problem this is, nevertheless, a crude approximation. We now apply the operator c_ν

$$\begin{aligned} c_\nu(|\Phi\rangle) &= c_\nu|1\rangle - \sum_\varepsilon \frac{V_{\nu\varepsilon}}{\Delta E_+ - \varepsilon} c_{\nu\varepsilon}|0\rangle \\ &- \sum_{\nu'(\neq\nu)} \sum_\varepsilon \frac{V_{\nu'\varepsilon}}{\Delta E_+ - \varepsilon} c_\nu c_{\nu'}^\dagger c_{\nu'\varepsilon}|1\rangle. \end{aligned} \quad (43)$$

The term $c_\nu|\Phi_{n_0-1}\rangle$ can be neglected for $U \gg |V|$. We form a final state

$$\begin{aligned} |\tilde{0}\rangle &= c_{\nu\varepsilon_F}(|0\rangle + |1\rangle) \\ &- \sum_\varepsilon \frac{V_{\nu\varepsilon}}{\Delta E_- + \varepsilon} c_{\nu\varepsilon}^\dagger c_\nu c_{\nu\varepsilon_F}|1\rangle, \\ &- \sum_{\nu'(\neq\nu)} \sum_\varepsilon \frac{V_{\nu'\varepsilon}}{\Delta E_- + \varepsilon} c_{\nu'\varepsilon}^\dagger c_{\nu'} c_{\nu\varepsilon_F}|\Phi_{n_0}\rangle). \end{aligned} \quad (44)$$

where $\varepsilon_F = 0$ is the Fermi energy. This state is closely related to the initial ground-state except for a hole at the Fermi energy. We use this as an approximation to the lowest final state. We could also have added a term corresponding to $n_0 + 1$ electrons on the cluster, but this would not have contributed to the matrix elements below. Then the amplitude for the photoemission process is

$$\begin{aligned} \langle \tilde{0}|c_\nu|\Phi\rangle &= \sum_\varepsilon V_{\nu\varepsilon} \left(\frac{\langle 1|c_{\nu\varepsilon_F}^\dagger c_{\nu\varepsilon}|1\rangle}{\Delta E_- + \varepsilon} - \frac{\langle 0|c_{\nu\varepsilon_F}^\dagger c_{\nu\varepsilon}|0\rangle}{\Delta E_+ - \varepsilon} \right) \\ &- \sum_{\nu'(\neq\nu)\varepsilon} V_{\nu'\varepsilon} \left(\frac{\langle 0|c_{\nu\varepsilon_F}^\dagger c_{\nu'}^\dagger c_{\nu'} c_{\nu\varepsilon}|1\rangle}{\Delta E_- + \varepsilon} + \frac{\langle 0|c_{\nu\varepsilon_F}^\dagger c_\nu c_{\nu'}^\dagger c_{\nu'\varepsilon}|1\rangle}{\Delta E_+ - \varepsilon} \right). \end{aligned} \quad (45)$$

If $(|0\rangle - |1\rangle)$ is an excited state of the cluster, we can form a final state analogous to Eq. (44) and obtain an expression for the weight similar to Eq. (45), except for some signs. In cases where there is a strong negative interference for the coupling to the lowest final state there might be a strong positive interference for the coupling to this satellite.

We can now discuss the problem of a cluster coupling to a large bath in the limit of very weak coupling. We first consider the case when a good zeroth order approximation is given by a direct product of the lowest cluster state and the bath filled up to the Fermi energy (no holes present), having the case in mind when the lowest cluster state is nondegenerate. The Ansatz in Eq. (44) for the lowest final state should then also be appropriate for a very large bath. To leading (zeroth) order in V/U the factor $\langle 1|c_{\varepsilon_F\nu}^\dagger c_{\varepsilon_F\nu}|1\rangle = \delta_{\varepsilon_F,\varepsilon} \langle 1|1\rangle$ in the first term in Eq. (45) and similar results for the second term. Similarly the term $c_{\varepsilon_F\nu}^\dagger c_{\varepsilon_F\nu'}$ ($\nu \neq \nu'$) acting on the bath in the third and fourth terms in Eq. (45) give zero contribution. To leading order in V/U the third and fourth terms are then zero and for the symmetric case the first and second term cancel. To leading order the lowest binding energy peak then has zero weight. This is schematically illustrated in Fig. 23a. The decisive point is that the matrix elements

$$\begin{aligned} \langle 0|H c_{\nu\varepsilon_F}^\dagger c_{\nu\varepsilon_F}|0\rangle &= V_{\nu\varepsilon_F} \\ \langle 1|c_{\nu\varepsilon_F}^\dagger H c_{\nu\varepsilon_F}|1\rangle &= -V_{\nu\varepsilon_F} \end{aligned} \quad (46)$$

have different signs. Then the two paths of reaching the final state have destructive interference.

If $(|0\rangle - |1\rangle)$ is an excited state of the isolated cluster, there is instead constructive interference for the final state $c_{\varepsilon_F\nu}(|0\rangle - |1\rangle)$, since the first and second terms in Eq. (45) now have the same sign.

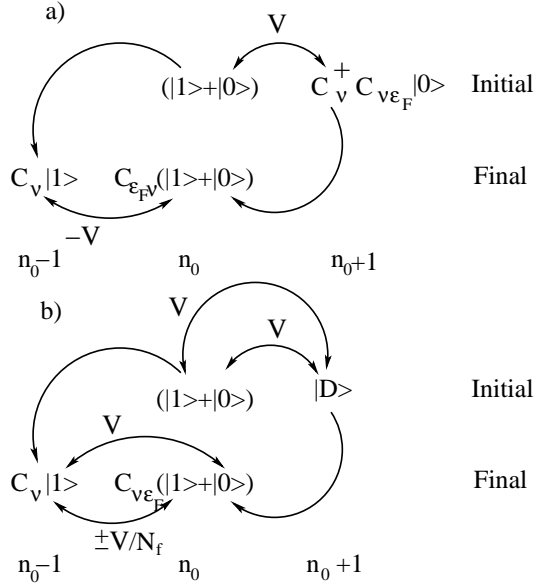


FIG. 23. Schematic illustration of initial and final states for the case when the lowest state $|0\rangle + |1\rangle$ of the isolated cluster is a) nondegenerate or b) degenerate in the $U \gg |V|$ limit. An electron with the quantum number ν is removed in a photoemission process. $|0\rangle$ contains no electron ν while $|1\rangle$ does. Figure a) (nondegenerate case) illustrates the negative interference between two channels for reaching the final state, corresponding to the two first terms in Eq. (45). Figure b) (degenerate case) illustrate how spin-flip terms (third and fourth terms in Eq. (45)) interfere positively with path going through double occupancy. D stands for doubly occupied states. The negative amplitude between $n_0 - 1$ and n_0 sectors of the final state is suppressed by $1/N_f$ with respect to positive spin-flip contributions leading to overall positive interference between different paths.

This kind of scenario may be expected when the lowest cluster state is nondegenerate and the bath is infinite. It is interesting to compare with the case $\Delta U > 0$ for the four-level model, since the isolated cluster ground-state is then nondegenerate. For this finite system the ground-state of the cluster plus bath [Eq. (36)] is more complicated than suggested above, even for $U \rightarrow \infty$. The model nevertheless illustrates the ideas above. Table VIII shows the calculated weight of the lowest binding energy peak (“Peak 1”) and the estimate according to Eq. (45). Indeed both weights are extremely small for a large value of U . In table VIII the terms occurring in Eq. (45) are explicitly evaluated showing the cancellation between the first and second terms explaining the vanishing weight of “Peak 1”. The estimate Eq. (45) is only correct to leading order in V/U , and to this order the weight is zero. The weight is then determined by higher order terms, which are not correct in Eq. (45) and, in addition, Eq. (45) refers to an infinite system. Nevertheless, the weight is of the right order of magnitude. Table VIII also shows the weight the peak corresponding to the final state $(|0\rangle - |1\rangle)$ (“Peak 3”) together with an estimate analo-

gous to Eq. (45). For very large values of U this estimate is fairly accurate, given that it was done assuming an infinite bath. The destructive interference at the lowest binding energy can also be understood in terms of phase shift arguments.⁵² However, the formalism used here contains additional information about the spectral weights of higher energy excitations determining the pseudogap.

The case $\Delta U < 0$ in the four-level model is quite different. In this case the ground-state is Kondo-like. To obtain a better understanding of this case, we study a simple model of Ce compounds,⁶⁸ based on the Anderson impurity model.

$$H = \sum_{\nu=1}^{N_f} \int_{-B}^B \varepsilon c_{\nu\varepsilon}^\dagger c_{\nu\varepsilon} d\varepsilon + \varepsilon_f \sum_{\nu=1}^{N_f} c_{\nu}^\dagger c_{\nu} + V \sum_{\nu=1}^{N_f} \int d\varepsilon (c_{\nu\varepsilon}^\dagger c_{\nu} + \text{h.c.}) + U \sum_{\nu < \nu'} n_{\nu} n_{\nu'}$$

Here the impurity has a N_f -fold degeneracy, including orbital and spin degeneracies. For the ground-state we have the basis states

$$\begin{aligned} |\phi_0\rangle &= \prod_{\varepsilon}^{\text{occ}} \prod_{\nu=1}^{N_f} c_{\nu\varepsilon}^\dagger |\text{vacuum}\rangle \\ |\varepsilon\rangle &= \frac{1}{\sqrt{N_f}} \sum_{\nu=1}^{N_f} c_{\nu}^\dagger c_{\nu\varepsilon} |\phi_0\rangle \\ |\varepsilon\varepsilon'\rangle &= \frac{1}{\sqrt{N_f(N_f-1)}} \sum_{\nu,\nu'} c_{\nu}^\dagger c_{\nu\varepsilon} c_{\nu'\varepsilon'}^\dagger |\phi_0\rangle \end{aligned} \quad (47)$$

For the states $|\varepsilon\varepsilon'\rangle$ we require that $\varepsilon > \varepsilon'$ to avoid over-completeness. In the limit of a very large N_f , the ground-state is written as⁶⁸

$$|\Phi\rangle = A \left(|\phi_0\rangle + \int_{-B}^0 d\varepsilon a(\varepsilon) |\varepsilon\rangle + \int_{-B}^0 d\varepsilon \int_{-B}^{\varepsilon} d\varepsilon' b(\varepsilon, \varepsilon') |\varepsilon\varepsilon'\rangle \right). \quad (48)$$

We remove an electron with quantum number ν . The relevant final state basis states are

$$\begin{aligned} |\tilde{\varepsilon}\rangle &= c_{\nu\varepsilon} |\phi_0\rangle \\ |\varepsilon\tilde{\varepsilon}'1\rangle &= \frac{1}{\sqrt{N_f-1}} \sum_{\nu' \neq \nu} c_{\nu'}^\dagger c_{\nu'\varepsilon'} c_{\nu\varepsilon} |\phi_0\rangle \\ |\varepsilon\tilde{\varepsilon}'2\rangle &= c_{\nu}^\dagger c_{\nu\varepsilon'} c_{\nu\varepsilon} |\phi_0\rangle, \end{aligned} \quad (49)$$

where $\varepsilon > \varepsilon'$ for the state $|\varepsilon\tilde{\varepsilon}'2\rangle$. To leading order in $(1/N_f)$ $|\varepsilon\tilde{\varepsilon}'2\rangle$ can be neglected, and to this order we can form a final state

$$|\varepsilon_F \text{final}\rangle = c_{\nu\varepsilon_F} |\Phi\rangle. \quad (51)$$

The overlap to the ground-state is then

$$\begin{aligned} \langle \varepsilon_F \text{final} | c_{\nu} | \Phi \rangle & \\ = \frac{A^2}{\sqrt{N_f}} \left(a(\varepsilon_F) + \sqrt{\frac{N_f-1}{N_f}} \int_{-B}^0 d\varepsilon a(\varepsilon) b(\varepsilon_F, \varepsilon) \right), & \end{aligned} \quad (52)$$

where $\epsilon_F = 0$ is assumed. Importantly, this expression shows positive interference, in contrast to what we found for the $\Delta U > 0$ four-level model. For instance, if $V < 0$ all coefficients A , a and b are positive. If the states $|\epsilon\tilde{\epsilon}'2\rangle$ are considered, it is not possible to write a final state in the simple form (51), and there are then also contributions to $|\langle\epsilon_F\text{final}|c_\nu|\Phi\rangle|^2$ with negative interference. These contributions are, however, one order higher in $(1/N_f)$.

We analyze the result as above, and form the states $|0\rangle$ and $|1\rangle$ as defined above[Eq. (38)].

$$\begin{aligned} |0\rangle &= \frac{A}{\sqrt{N_f}} \int_{-B}^0 d\epsilon a(\epsilon) \sum_{\nu'(\neq\nu)} c_{\nu'}^\dagger c_{\nu'\epsilon} |\phi_0\rangle \\ |1\rangle &= \frac{A}{\sqrt{N_f}} \int_{-B}^0 d\epsilon a(\epsilon) c_{\nu\epsilon}^\dagger |\phi_0\rangle. \end{aligned} \quad (53)$$

It turns out that the second to fourth terms in Eq. (45) give the leading contributions in $(1/N_f)$, and therefore we first consider the second term in the limit when $-\epsilon_f \gg B$. Since $|0\rangle$ has no holes with quantum number ν below ϵ_F , this term only contributes for $\epsilon = \epsilon_F$. Then we have

$$\begin{aligned} & - \sum_{\epsilon} V \frac{\langle 0 | c_{\nu\epsilon}^\dagger c_{\nu\epsilon} | 0 \rangle}{U + \epsilon_f - \epsilon_F} \\ &= - \frac{A^2(N_f - 1)}{N_f} \frac{V}{U + \epsilon_f - \epsilon_F} \int_{-B}^0 d\epsilon a(\epsilon)^2. \end{aligned} \quad (54)$$

This corresponds to the process $|0\rangle \rightarrow |D\rangle \rightarrow c_{\nu\epsilon_F}|0\rangle$ in Fig. 23. The matrix element of the Hamiltonian is proportional to V and the removal of the electron ν does not involve a minus sign. Next we consider the third term in Eq. (45).

$$\begin{aligned} & - \sum_{\nu'(\neq\nu)} \int_{-B}^0 d\epsilon V \frac{\langle 0 | c_{\nu\epsilon}^\dagger c_{\nu'\epsilon}^\dagger c_{\nu'\epsilon} c_{\nu\epsilon} | 1 \rangle}{-\epsilon_f + \epsilon} \\ &= - \frac{A^2(N_f - 1)V}{N_f} \int_{-B}^0 d\epsilon \frac{1}{-\epsilon_f + \epsilon} a(\epsilon)a(\epsilon_F) \end{aligned} \quad (55)$$

This term corresponds to the transition $|1\rangle \rightarrow c_\nu|1\rangle \rightarrow c_{\nu\epsilon_F}|0\rangle$. It describes spin flips and it has no correspondence for the nondegenerate case. It shows how the initial cluster neutral state with an electron ν is connected to a final cluster neutral state with an electron $\nu' \neq \nu$ via an intermediate state with no electron on the cluster. In the same way the fourth term describes a spin-flip term connecting initial and final neutral states via a doubly occupied state. As in Eq. (54), the matrix element of the Hamiltonian is in both cases proportional to V and the removal of the electron ν does not involve a minus sign. These two terms interfere positively with each other and with the second term.

Finally, we consider the first term in Eq. (45).

$$\begin{aligned} & \int_{-B}^0 d\epsilon \frac{V}{-\epsilon_f + \epsilon} \langle 1 | c_{\nu\epsilon}^\dagger c_{\nu\epsilon} | 1 \rangle \\ &= \frac{A^2V}{N_f} \left(\frac{1}{-\epsilon_f + \epsilon_F} \int_{-B}^{0^-} d\epsilon a^2(\epsilon) - \int_{-B}^{0^-} d\epsilon \frac{1}{-\epsilon_f + \epsilon} a(\epsilon)a(\epsilon_F) \right) \end{aligned} \quad (56)$$

The state $c_{\nu\epsilon_F}|1\rangle$ corresponds to the final basis state $|\epsilon\tilde{\epsilon}'2\rangle$. Coupling to the $n_0 - 1$ state, the cluster electron can now fill one out of two holes for $\epsilon \leq \epsilon_F$. This differs from the states we considered in the nondegenerate state, where there was only one hole. If the hole at ϵ_F is filled, the sign is the same as in the nondegenerate case, and a negative interference with the following three terms in Eq. (45) is obtained, due to the commutations of fermion operators. If instead the other hole is filled, a constructive interference is obtained. Both terms in Eq. (56) are one order smaller in $(1/N_f)$ than the following terms in Eq. (45). Therefore there is in total a strong constructive interference.

This is illustrated in Table VIII for the case $\Delta U < 0$. For large values of U the theory above describes accurately the weight of the lowest binding energy peak. In this case $|0\rangle - |1\rangle$ is not a proper excited state. Actually, it is not even orthogonal to $|0\rangle + |1\rangle$. Therefore we have no simple estimate of the weight of the third peak in this case.

We can now analyze a $N_c = 4$ DCA calculation in the light of the results above. Fig. 24 shows some results. We first consider the correlation functions $C_{(\pi,0)\uparrow(\pi,0)\downarrow}$, $C_{(\pi,0)\uparrow(0,\pi)\uparrow}$, $C_{(\pi,0)\uparrow(0,\pi)\downarrow}$, defined as in Eq. (14). The correlation function $C_{(\pi,0)\uparrow(\pi,0)\downarrow}$ shows how initially for small U there is a negative correlation between spin up and spin down electrons in the $(\pi,0)$ orbital. This corresponds to a Kondo like coupling of each orbital to its bath and a large amplitude $A(\omega = 0)$ of the peak at the Fermi energy. This is also illustrated by

$$G(\tau = \beta/2) = \int_{-\infty}^{\infty} \frac{e^{-\beta\omega/2}}{1 + e^{-\beta\omega}} A(\omega) d\omega, \quad (57)$$

which gives an average of $A(\omega)$ around $\omega = 0$ over an energy range of the order of πT . As U increases, $C_{(\pi,0)\uparrow(\pi,0)\downarrow}$ turns positive and at the same time $C_{(\pi,0)\uparrow(0,\pi)\uparrow}$ and $C_{(\pi,0)\uparrow(0,\pi)\downarrow}$ become very negative. This is the correlation also observed for the four-level model in Fig. 21 and it corresponds to the formation of a cluster singlet where the main configuration is

$$\frac{1}{\sqrt{2}} [c_{(\pi,0)\uparrow}^\dagger c_{(\pi,0)\downarrow}^\dagger - c_{(0,\pi)\uparrow}^\dagger c_{(0,\pi)\downarrow}^\dagger] c_{(0,0)\uparrow}^\dagger c_{(0,0)\downarrow}^\dagger |\text{vacuum}\rangle, \quad (58)$$

equivalent to the ground-state of the four-level model, except for the additional double occupation of $\mathbf{k} = (0,0)$. At this point the peak weight drops dramatically, shown by both $A(\omega = 0)$ and $G(\tau = \beta/2)$.

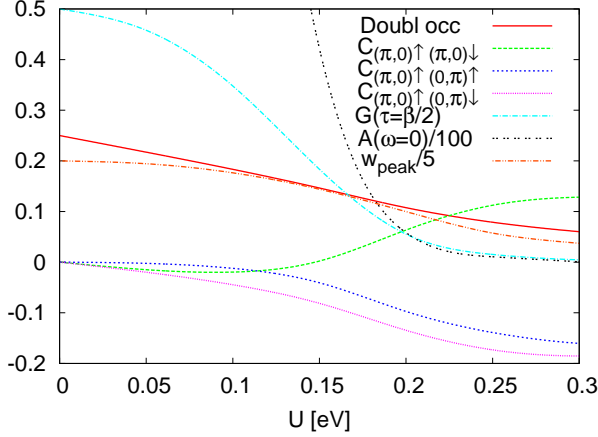


FIG. 24. DCA results for a four site cluster. The double occupancy, $C_{(\pi,0)\uparrow(\pi,0)\downarrow}$, $C_{(\pi,0)\uparrow(0,\pi)\uparrow}$, $C_{(\pi,0)\uparrow(0,\pi)\downarrow}$ [defined as in Eq. (14)], $G(\tau = \beta/2)$, $A(\omega = 0)/100$ and the weight w_{peak} of the peak within 0.05 eV of the Fermi energy are shown. The parameters are $t = -0.04$ eV, $t' = 0$ and $T = 29$ K. The results were obtained after the first iteration.

The figure also shows the weight w_{peak} of the peak integrated over a range ± 0.05 eV around the Fermi energy. This corresponds to the drop described in Sec. IV for the two-level model. As U is increased the double occupancy is reduced. As described in Fig. 18 the coupling to neutral final cluster states is then weaker and there is less weight close to the Fermi energy. Correspondingly the interaction in the final states between charged and neutral final configurations is weaker. This reduces the weight w_{peak} . This is, however, just a part of the physics. More important are the interference effects discussed in this section. When the dominating part of the ground-state starts to become a nondegenerate state on the cluster, interference effects move weight from the Fermi energy to side bands relatively close to the Fermi energy (much closer than the Hubbard side bands) but away from the Fermi energy. This is illustrated in Fig. 24, by the much faster drop by $G(\tau = \beta/2)$ and, in particular, $A(\omega = 0)$.

VII. EIGHT SITE CLUSTER

A. Unfrustrated case

As seen in, eg., Fig. 14, the embedded eight-site cluster gives a pseudogap for $\mathbf{K} = (\pi, 0)$ but no pseudogap for $\mathbf{K} = (\pi/2, \pi/2)$ for intermediate values of U/W . This is also the case for the first iteration. We now discuss the physics of this in relation to the results of the previous sections. Fig. 25 shows correlation functions defined as in Eq. (14). We first consider $C_{(\pi,0)\uparrow(\pi,0)\downarrow}$ (full red curve). In analogy with $C_{(\pi,0)\uparrow(\pi,0)\downarrow}$ in Fig. 24 for the four-site cluster, the curve first turns negative, indicating that a Kondo state is formed. For U of the order of 0.24 eV it turns positive, indicating the formation of a localized

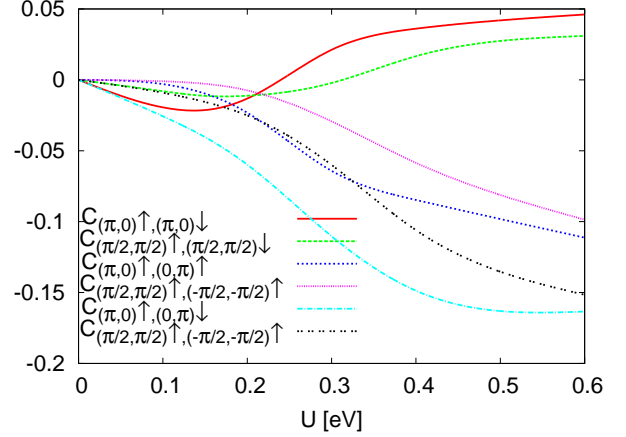


FIG. 25. Correlation functions C_{ij} defined in analogy to Eq. (14) as a function of U for an eight site cluster. The parameters are $t = -0.04$ eV, $t' = 0$ and $T = 29$ K. The results were obtained in the first iteration.

state in the cluster, again in analogy with the four-site cluster. The correlation of $\mathbf{K} = (\pi, 0) \uparrow$ to $\mathbf{K} = (0, \pi) \uparrow$ or \downarrow is strongly negative, also as for the four-site cluster. We next focus on the correlation between $\mathbf{K} = (\pi/2, \pi/2) \uparrow$ and $\mathbf{K} = (\pi/2, \pi/2) \downarrow$ (dotted green curve). This curve behaves in a similar way as the corresponding curve for $\mathbf{K} = (\pi, 0)$ but it is displaced towards higher values of U . This is easy to understand in terms of the stronger coupling to the bath for $\mathbf{K} = (\pi/2, \pi/2)$ than for $\mathbf{K} = (\pi, 0)$, illustrated in, e.g., Fig. 2. This stronger coupling makes it favorable to keep a Kondo like state for $\mathbf{K} = (\pi/2, \pi/2)$ up to a larger value of U . For still large values of U , however, it is more favorable to form a localized cluster state also for this \mathbf{K} value.

For the four-site cluster, only the $(\pi, 0)$ and $(0, \pi)$ levels are available at the Fermi energy. It is then not surprising that these form a localized state for larger values of U , as in the four-level model. For the eight-site cluster, on the other hand, also the $(\pm\pi/2, \pm\pi/2)$ levels are available. One may then ask to what extent the $(\pi, 0)$ and $(0, \pi)$ levels can form a localized state without involving the $(\pm\pi/2, \pm\pi/2)$ levels. This is illustrated in Fig. 26. For $U \leq 0.24$ eV, where $C_{(\pi,0)\uparrow(\pi,0)\downarrow}$ is negative, there is essentially no correlation between $(\pi, 0)$ and $(\pm\pi/2, \pm\pi/2)$ for equal spin, while there is a negative coupling for different spins. The Kondo-like states in the $(\pi, 0)$ and $(\pm\pi/2, \pm\pi/2)$ channels are therefore not completely independent as was also observed for the Kondo-like states in the $(\pi, 0)$ and $(0, \pi)$ channels. For $0.24 < U < 0.31$ eV, where the localized state in the $(\pi, 0) - (0, \pi)$ space starts to form, the unequal spin correlation function $C_{(\pi,0)\uparrow(\pi/2,\pi/2)\downarrow}$ becomes small. Here the correlation between $(\pi, 0)$ and $(\pm\pi/2, \pm\pi/2)$ is indeed rather weak, and a similar localized state forms as for the four-site cluster. For $U > 0.31$ eV a localized state starts to form also in the $(\pm\pi/2, \pm\pi/2)$ space. Now the correlation between the two spaces is substantial for

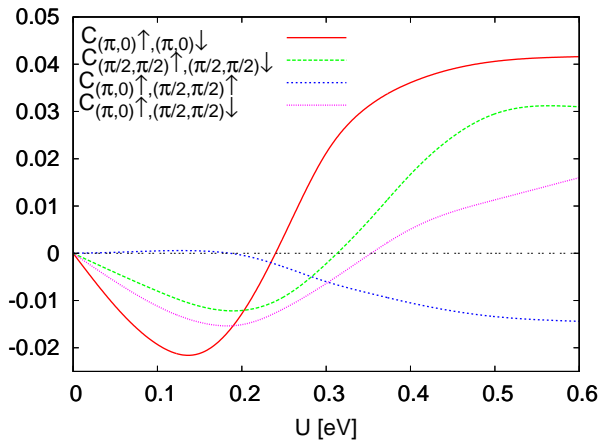


FIG. 26. Correlation functions C_{ij} between the $(\pi, 0)$ and $(\pi/2, \pi/2)$ states [Eq. (14)] as a function of U for an eight site cluster. The parameters are $t = -0.04$ eV, $t' = 0$ and $T = 29$ K. The results were obtained in the first iteration.

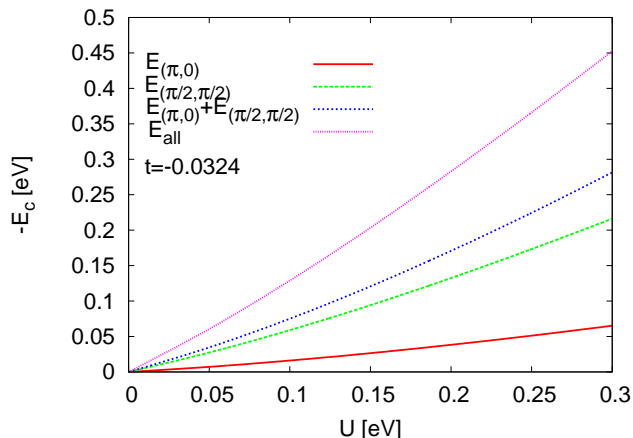


FIG. 27. Correlation energy for an isolated eight site cluster. Results are shown for the case when the $(\pm\pi/2, \pm\pi/2)$ states are not allowed to participate in the correlation [referred to as “ $(\pi, 0)$ ”] or the $(\pi, 0)$ and $(0, \pi)$ states are not allowed to correlate [referred to as “ $(\pi/2, \pi/2)$ ”] or when all states are involved in the correlation (referred to as “all”). The difference between E_{all} and $E_{(\pi,0)} + E_{(\pi/2, \pi/2)}$ curves quantifies the energy gain from the correlation between $(\pi, 0)$ and $(\pm\pi/2, \pm\pi/2)$ electrons. The parameters are $t_{cluster} = -0.0324$ eV, $t' = 0$ and $T = 0$.

both equal and unequal spins. This is discussed below.

Given the large difference in the coupling to the bath, it may seem surprising that the localization of the $(\pi/2, \pi/2)$ electrons does not happen for an even larger value of U . To understand this we discuss the gain in correlation energy when electrons localize on the cluster.

Fig. 27 shows correlation energies for an isolated eight site cluster as a function of U . The curve $E_{(\pi,0)}$ was obtained by including just four electrons and putting the $(\pm\pi/2, \pm\pi/2)$ levels at very high energies. This corresponds to nominally occupy the $\mathbf{K} = (0, 0)$ level

doubly and then allowing the remaining two electrons to correlate in the $(\pi, 0)$ and $(0, \pi)$ states. Then the $(\pm\pi/2, \pm\pi/2)$ levels do not participate in the correlation process. This may crudely represent the situation when the $(\pm\pi/2, \pm\pi/2)$ electrons form Kondo states with the bath but the $(\pi, 0)$ and $(0, \pi)$ electrons have localized. The latter electrons can then correlate internally, while the $(\pm\pi/2, \pm\pi/2)$ electrons primarily optimize the interaction with the bath and correlate less efficiently with the $(\pi, 0)$ and $(0, \pi)$ electrons, as discussed above. Although there are nominally two electrons in the $\mathbf{K} = (0, 0)$ level, these electrons are allowed to fully correlate with the other two electrons, and the $\mathbf{K} = (\pi, \pi)$ orbital also participates. For the curve $E_{(\pi/2, \pi/2)}$ we have instead put the $(\pi, 0)$ and $(0, \pi)$ at very high energy and we now include six electrons, nominally two electrons in the $\mathbf{K} = (0, 0)$ level and the remaining four electrons nominally in the $(\pm\pi/2, \pm\pi/2)$ orbitals. E_{all} is obtained by calculating the correlation energy without any constraints for eight electrons. This would correspond to all eight electrons being roughly localized in the cluster.

We also show $E_{(\pi,0)} + E_{(\pi/2, \pi/2)}$. This sum involves some double counting, since in one case the orbitals $\mathbf{K} = (0, 0)$ and $\mathbf{K} = (\pi, \pi)$ can fully correlate with the $(\pi, 0)$ and $(0, \pi)$ electrons and in the other with the $(\pm\pi/2, \pm\pi/2)$ electrons. Nevertheless, this curve is much lower than E_{all} . This shows that a lot of correlation energy is gained by allowing the $(\pi, 0)$ and $(0, \pi)$ electrons to correlate with the $(\pm\pi/2, \pm\pi/2)$ electrons, which is not included in the sum $E_{(\pi,0)} + E_{(\pi/2, \pi/2)}$. This is also illustrated by the substantial correlation between $(\pi, 0)$ and $(\pm\pi/2, \pm\pi/2)$ in Fig. 26 for large U . This gives a strong tendency for all electrons to localize simultaneously, since then particularly much energy can be gained. The difference in the values of U where the curves in Fig. 26 turn upwards for the $(\pi, 0)$ and $(\pm\pi/2, \pm\pi/2)$ channels is therefore substantially smaller than one would expect from the differences in the couplings (factor of 3-4). Nevertheless, the upturn does happen for a larger U in the $(\pm\pi/2, \pm\pi/2)$ channel, and therefore there is a pseudogap in $(\pi, 0)$ but not in $(\pm\pi/2, \pm\pi/2)$ for intermediate values of U .

B. Frustrated case

So far we have considered the unfrustrated case when $t' = 0$. We now put in frustration, $t' = -0.3t$, which is more appropriate for cuprates. The results are shown in Fig. 28 for different fillings. Fig. 28a shows a hole-doped case (doping 8.5%). This shows a clear pseudogap for $\mathbf{K} = (\pi, 0)$. For the approximately half-filled case ($n = 0.997$) (Fig. 28b) there is no pseudogap. Increasing the filling further to $n = 1.086$ (Fig. 28c) the filling of the $\mathbf{K} = (\pi, 0)$ level is substantially increased, but otherwise the spectral function is not changed much and no pseudogap is formed. These results were obtained in the first iteration. Self-consistent calculations also

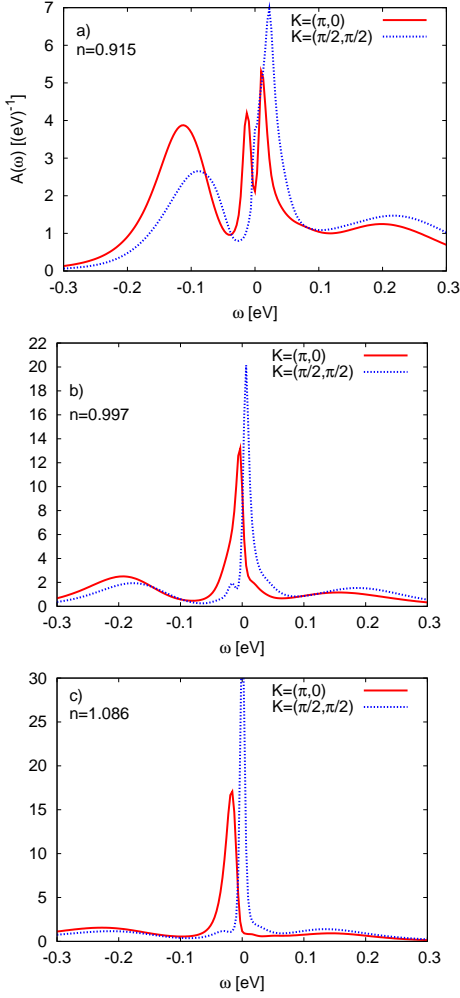


FIG. 28. Spectral function for different fillings. The parameters are $t = -0.04$ eV, $t' = 0.12$ eV, $U = 0.32$ eV and $T = 38.4$ K. First iteration results are plotted.

show a pseudogap for the hole-doped case but not for the electron-doped case, but there are differences in the doping dependence. For instance, in the self-consistent case the pseudogap becomes very pronounced for small hole-dopings.

This difference between electron- and hole-doping has been observed experimentally.⁷⁵ Experimentally, the electron-doped sample is antiferromagnetic for the parameters considered here, while the calculations show that the $(\pi, 0)$ pseudogap also disappears for the paramagnetic calculation.²⁰ It is then particularly interesting to study the paramagnetic state, to see why just a small change in the chemical potential removes the $(\pi, 0)$ pseudogap.

To further illustrate the difference between hole- and electron-doped systems, we show correlation functions in Fig. 29 also studied earlier for $t' = 0$. For the hole-doped system, the $C_{(\pi,0)\uparrow(\pi,0)\downarrow}$ correlation function has a fairly large positive value, indicating that a localized state has formed in the $(\pi, 0)$ - $(0, \pi)$ space. As the filling

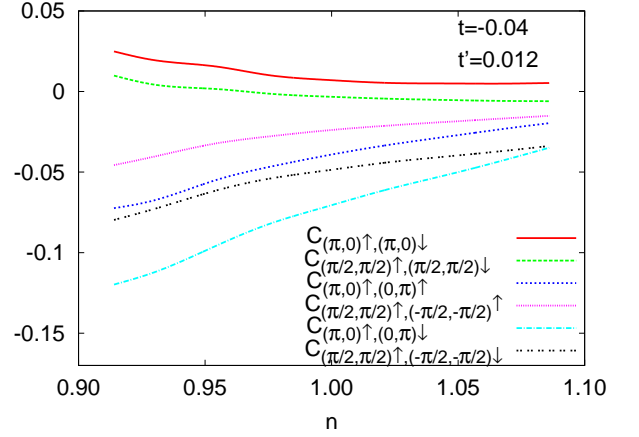


FIG. 29. Correlation functions C_{ij} defined in analogy to Eq. (14) as a function of the filling n for a frustrated eight site cluster. The parameters are $U = 0.32$ eV, $t = -0.04$ eV, $t' = 0.012$ eV and $T = 38.4$ K. The parameter n_0 [Eq. (2)] was chosen as $n/2$. The results were obtained after the first iteration.

is increased, this correlation function is reduced, indicating that the tendency to form a localized cluster state is weakened. The correlation function $C_{(\pi/2,\pi/2)\uparrow(\pi/2,\pi/2)\downarrow}$ is weakly positive for a substantial hole doping, but apparently not enough to cause a pseudogap. This function is also reduced with increasing filling and becomes negative for electron-doping. We now analyze the reasons for the difference between hole-doped and electron-doped systems.

1. Exact diagonalization

To obtain additional understanding we perform exact diagonalization (ED) calculations. We analyze the doping dependence of the $N_c = 8$ clusters coupled to a bath described by $N_b = 8$ bath states. This coupling was held fixed as the chemical potential is varied. We have evaluated spin correlations and hybridization energies between cluster and bath electrons to quantify the strength of antiferromagnetic correlations associated with the Kondo effect. We evaluate the hybridization energy from the expression:

$$\langle V(\mathbf{K}) \rangle = \sum_{\mathbf{k}\sigma} V(\mathbf{K}) (\langle c_{\mathbf{K},\sigma}^\dagger c_{\mathbf{K}+\mathbf{k},\sigma} \rangle + \langle c_{\mathbf{K}+\mathbf{k},\sigma}^\dagger c_{\mathbf{K},\sigma} \rangle), \quad (59)$$

where $c_{\mathbf{K}\sigma}^\dagger$ and $c_{\mathbf{K}+\mathbf{k}\sigma}^\dagger$ creates an electron on the cluster or in the bath, respectively. Here the sum over \mathbf{k} is reduced to one value. We also calculate the correlation between a spin $S_z(\mathbf{K})$ in the cluster and the spin of its bath level $s_z(\mathbf{k})$.

For the half-filled unfrustrated case, $t' = 0$, the various spin correlations and hybridization energies are given in Table IX. It is found that the hybridization energy

TABLE IX. Bath-cluster spin correlations and hybridization energies from ED calculations on $N_b = N_c = 8$ clusters at half-filling ($n = 1$). The z -component of the spin of a bath (cluster) electron in, for instance, the $(\pi, 0)$ channel is denoted by $s_z(\pi, 0)$ [$S_z(\pi, 0)$]. The cluster bath couplings are $V(\pi, 0) = 0.008$ eV and $V(\pi/2, \pi/2) = 0.021$ eV. We take $t = -0.04$ eV, $t' = 0$ for $U = 0.25$ eV and $U = 0.32$ eV.

U	μ	$\langle S_z(\mathbf{K})s_z(\mathbf{k}) \rangle$		$\langle V(\mathbf{K}) \rangle$	
		$(\pi, 0)$	$(\frac{\pi}{2}, \frac{\pi}{2})$	$(\pi, 0)$	$(\frac{\pi}{2}, \frac{\pi}{2})$
0.25	0.125	-0.0020	-0.0051	-0.0021	-0.0097
0.32	0.160	-0.0012	-0.0030	-0.0014	-0.0066

TABLE X. Bath-cluster spin correlations and hybridization energies from exact diagonalization calculations on $N_b = N_c = 8$ frustrated clusters. There is one bath level per cluster orbital at the Fermi energy with the bath cluster couplings fixed at $V(\pi, 0) = 0.008$ eV and $V(\pi/2, \pi/2) = 0.021$ eV. We also show $J_K(\mathbf{K})$ calculated according to Eq. (60). The parameters are $t = -0.04$ eV, $t' = -0.3t$ and $U = 0.25$ eV.

μ	n	$\langle S_z(\mathbf{K})s_z(\mathbf{k}) \rangle$		$\langle V(\mathbf{K}) \rangle$		$J_K(\mathbf{K})/ V(\mathbf{K}) ^2$	
		$(\pi, 0)$	$(\frac{\pi}{2}, \frac{\pi}{2})$	$(\pi, 0)$	$(\frac{\pi}{2}, \frac{\pi}{2})$	$(\pi, 0)$	$(\frac{\pi}{2}, \frac{\pi}{2})$
0.085	0.96	-0.0042	-0.0068	-0.0036	-0.012	16.1	17.8
0.105	0.98	-0.0038	-0.0063	-0.0035	-0.011	16.9	16.4
0.125	1.00	-0.0048	-0.0065	-0.0043	-0.011	18.8	16.0
0.135	1.02	-0.0064	-0.0063	-0.0047	-0.012	20.4	16.1
0.145	1.04	-0.0084	-0.0071	-0.0055	-0.013	22.7	16.4

is smaller for $(\pi, 0)$ than $(\pi/2, \pi/2)$ as it should, since the coupling is smaller for $(\pi, 0)$. The spin correlation $\langle S_z(\mathbf{K})s_z(\mathbf{k}) \rangle$ is negative, as for the four-level model in Fig. 21. This correlation is more negative for $(\pi/2, \pi/2)$ than for $(\pi, 0)$, due to the stronger cluster-bath coupling. Increasing U leads to a suppression of the spin correlations as one would expect, since the Kondo couplings are suppressed and it becomes more favorable to correlate the electrons inside the cluster. This supports the conclusions above.

The dependence of the spin correlations on doping is summarized in Table X for the frustrated case ($t' = -0.3t$). In the $(\pi, 0)$ channel the cluster-bath antiferromagnetic spin correlations and the hybridization energy increase with the filling, moderately on the hole-doped side and more strongly on the electron-doped side. In the $(\pi/2, \pi/2)$ channel, on the other hand, these quantities vary little with filling in the range considered, with a tendency to a minimum at $n = 1$.

In order to rationalize the doping dependence of the antiferromagnetic Kondo correlations, we have estimated the Kondo couplings obtained from a Schrieffer-Wolff transformation of the Anderson Hamiltonian:

$$J_K(\mathbf{K}) = |V(\mathbf{K})|^2 \left(\frac{1}{\epsilon(\mathbf{K}) + U - \mu} + \frac{1}{\mu - \epsilon(\mathbf{K})} \right). \quad (60)$$

This estimate should be relevant when the correlation between different \mathbf{K} levels on the cluster is weak and the

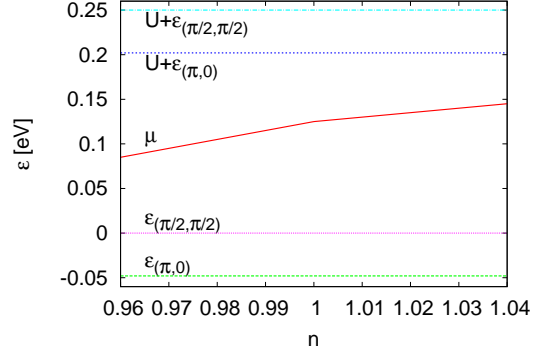


FIG. 30. Energy levels and chemical potential relevant for the calculation of the Schrieffer-Wolff exchange coupling, J_K .

coupling to the bath dominates. The results are shown in Table X. $J_K(\pi, 0)$ increases in going from the hole-doped to the electron-doped side, as found for the spin correlations. $J_K(\pi/2, \pi/2)$ varies little with a weak minimum at $n = 1$. This is also in line with the results for the spin correlations. The hybridization energy varies in a similar way as the spin correlations. This is not surprising, since the Schrieffer-Wolff exchange coupling, J_K , is derived from hopping between the cluster and the bath, as can also be seen from Eq. (60). The variation of J_K with filling can be understood from the energies shown in Fig. 30. For lower range of fillings considered here, the chemical potential μ is almost in the middle between the levels $\epsilon(\mathbf{K})$ and $U + \epsilon(\mathbf{K})$ for $\mathbf{K} = (\pi, 0)$. As the filling is increased μ moves upwards and gets much closer to $U + \epsilon(\mathbf{K})$. This favors a large J_K [Eq. (60)]. These arguments show that there is a substantial difference for the frustrated lattice and $\mathbf{K} = (\pi, 0)$ between the hole-doped and electron-doped systems. It is also interesting that if the sign of t' had been the opposite, as for the organics, this effect would have favored a pseudogap for the electron-doped systems. For $\mathbf{K} = (\pi/2, \pi/2)$ μ is roughly in the middle for $n = 1$ and is closer to one of the two levels for other fillings, giving a minimum in J_K at $n = 1$. In these ED calculations we held the coupling between the cluster and the bath fixed as μ was varied. This is an approximation, as can be seen from Eq. (8). Below we study μ dependence of the coupling.

2. μ dependence of the coupling strength

To discuss the dependence of the cluster-bath coupling $\Gamma_{\mathbf{K}}(\omega_n)$ on μ (or n) we use Eq. (7). As before we consider the first iteration when $\Sigma_c \equiv 0$. Then

$$\text{Im}\Gamma_{\mathbf{K}}(\omega_n) = \frac{\text{Im}G_0(\omega_n, \mathbf{K})}{[\text{Re}G_0(\omega_n, \mathbf{K})]^2 + [\text{Im}G_0(\omega_n, \mathbf{K})]^2} + \omega_n. \quad (61)$$

From Eqs. (4, 6) it follows that $\text{Im}G_0(\omega_n \rightarrow 0, \mathbf{K}) \sim N_{\mathbf{K}}(-\Delta)$, where $N_{\mathbf{K}}(\epsilon)$ is the sector density of states..

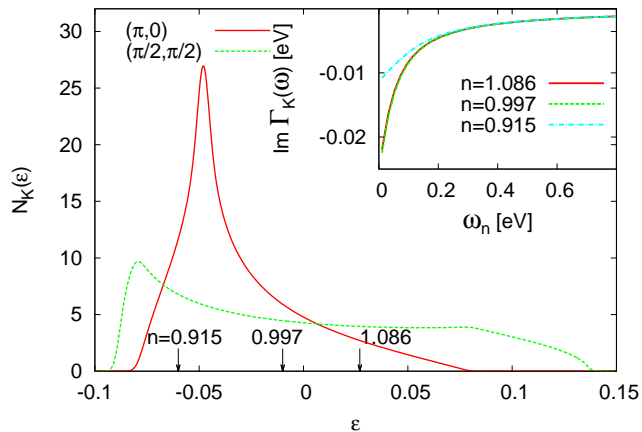


FIG. 31. The $\mathbf{K} = (\pi, 0)$ and $(\pi/2, \pi/2)$ sector density of states $N_{\mathbf{K}}(\varepsilon)$. The arrows show the values of $-\Delta = -Un_0 + \mu$ [Eq. (5)] for the different values of the filling n . The inset shows $\text{Im } \Gamma_{\mathbf{K}}(\omega_n)$ for different values of n . The parameters are $t = -0.04$ eV, $t' = 0.012$ eV, $U = 0.32$ eV and $T = 38.4$ K. First iteration results were used.

Fig. 31 shows the $N_{\mathbf{K}}(\varepsilon)$, and the arrows mark the positions of $-\Delta$ for different values of the filling n . For $n = 0.915$ it is clear that $\text{Im } G_0[\omega_n, (\pi, 0)]$ is large. Since $-\Delta$ is very asymmetrically located with respect to the center of gravity of $N_{\mathbf{K}}(\varepsilon)$ also $|\text{Re}G_0[\omega_n, (\pi, 0)]|$ is large. Then it follows from Eq. (61) that $\text{Im } \Gamma_{(\pi, 0)}(\omega_n \rightarrow 0)$ is small. For $n = 0.997$ and, in particular, $n = 1.086$, $\text{Im } G_0[\omega_n, (\pi, 0)]$ is smaller. $|\text{Re}G_0[\omega_n, (\pi, 0)]|$ is also smaller. This leads to a larger $\text{Im } \Gamma_{(\pi, 0)}(\omega_n \rightarrow 0)$, where numbers happen to combine in such a way that $\text{Im } \Gamma_{(\pi, 0)}(\omega_n \rightarrow 0)$ is very similar for $n = 0.997$ and $n = 1.086$. This is shown by the inset in Fig. 31. The curves for $n = 0.997$ and $n = 1.086$ fall almost on top of each other. The specific numbers for G_0 for $\omega_n = 0.0105$ eV are $(-22.0, -31.8)$, $(14.8, -18.8)$ and $(14.1, -9.2)$ for $n = 0.915, 0.997, 1.086$, respectively. For large ω_n , $\Gamma_{\mathbf{K}}$ is determined by the second moment of the sector density of states [Eq. (9)]. Therefore $\text{Im } \Gamma_{\mathbf{K}}(\omega_n)$ is very similar for all fillings in this limit.

We are now in the position to understand the behavior of the $\mathbf{K} = (\pi, 0)$ spectrum for the frustrated system as a function of filling. Starting out at small fillings ($n \sim 0.92$), both J/V^2 and $\text{Im } \Gamma_{\mathbf{K}}(\omega_n \rightarrow 0)$ are small for $\mathbf{K} = (\pi, 0)$, favoring a pseudogap. For filling one, J/V^2 increases somewhat and $\text{Im } \Gamma_{\mathbf{K}}(\omega_n \rightarrow 0)$ increases substantially. At the same time the pseudogap disappears. For still larger filling ($n = 1.086$), J/V^2 increases substantially and $\text{Im } \Gamma_{\mathbf{K}}(\omega_n \rightarrow 0)$ stays approximately constant for $\mathbf{K} = (\pi, 0)$. This further suppresses the pseudogap. This is supported by the results in Figs. 28, 29.

VIII. CHARACTER OF THE PSEUDOGAP

To study the character of the pseudogap we have studied the ground-state and excited states of a neutral isolated cluster. We have used the hopping integral $t_{\text{cluster}} = -0.0324$ eV, corresponding to $t = -0.04$ eV in DCA for $N_c = 8$. In the pseudogap phase the electrons in the $(\pm\pi/2, \pm\pi/2)$ levels are primarily correlated with the electrons in their baths and rather uncorrelated with electrons in the $(\pi, 0)$ and $(0, \pi)$ levels (see Fig. 26). Here we then assume that the two sets of electrons are completely uncorrelated and focus on the properties of the electrons in the $(\pi, 0)$ and $(0, \pi)$ levels. For this purpose we put the $(\pm\pi/2, \pm\pi/2)$ at some extremely high energy and then treat an isolated molecule with just four electrons. This then correspond to the nominally two electrons in the $(0, 0)$ level and two electrons in the $(\pi, 0)$ and $(0, \pi)$ levels. The four electrons nominally in the $(\pm\pi/2, \pm\pi/2)$ are not included in the calculation. This then approximately describes the pseudogap situation where the $(\pm\pi/2, \pm\pi/2)$ electrons are delocalized and the $(\pi, 0)$ and $(0, \pi)$ electrons are localized. The results are shown in Table XI. For the dominating configurations for the states shown in Table XI the level $(0, 0)$ is doubly occupied. The filling of the $(\pi, 0)$ and $(0, \pi)$ levels is similar as in Eq. (34) for the four lowest states. We have also calculated the pairing correlation P_d defined in Eq. (12) for the $x^2 - y^2$ symmetry.

We now consider photoemission, where an electron is emitted from the cluster. The spectral weight close to the Fermi energy then corresponds to low-lying final states, which are primarily composed of neutral cluster states. We can think of this as an electron hopping in from the bath after the photoemission process to obtain a neutral cluster. Since the lowest state has $S = 0$, removing an electron couples to $S = 1/2$ states. An electron hopping in from the bath then couples to $S = 0$ or $S = 1$ states. The relevant final states should then primarily be composed of such states. The peak to peak size of pseudogap in Fig. 14 is approximately 0.02 eV (for $U = 0.3$ eV). This then approximately corresponds to a transition to the second state in Table XI, giving a gap of about $2(0.1744 - 0.1632) = 0.022$ eV. The lowest state has large $d_{x^2-y^2}$ pairing fluctuations, while the first excited state has a negative P_d . We can then interpret the pseudogap as resulting from the break up of a local $d_{x^2-y^2}$ singlet state. We note that these are very short-range correlations, which may not be observable in experiment.

Here we have considered ratios of $U/|t| \sim 10$, close to a Mott transition, where the splitting of the states in Table XI depend rather weakly on $U/|t|$ for fixed t . These splittings are much larger than the values for the pseudogap in Ref. 52. However, the latter were obtained for much larger values of U/t . For such large values of $U/|t|$ the splittings in Table XI would go as $1/U$.

As a comparison, Table XII shows a calculation where the $(\pm\pi/2, \pm\pi/2)$ levels are not suppressed and the number of electrons is eight, as in a neutral cluster. This is

TABLE XI. Energy E , spin S and superconductivity correlation P_d for low-lying states with $S_z = 0$ for an isolated cluster with $N_c = 8$ and $T = 0$. The $(\pm\pi/2, \pm\pi/2)$ levels are artificially put at very high energy and effectively not part of the calculation. The number of electrons is four. The parameters are $U = 0.3$, $t_{\text{cluster}} = -0.0324$ eV and $t' = 0$.

E	S	P_d
-0.1744	0	0.69
-0.1632	1	-0.19
-0.1160	0	-0.19
-0.0824	0	-0.25

TABLE XII. Energy E , spin S , degeneracy Deg. and superconductivity correlation P_d for low-lying states with $S_z = 0$ for an isolated cluster with $N_c = 8$ and $T = 0$. All levels are included and there are eight electrons. Deg. refers to the degeneracy of $S_z = 0$ states. P_d for the state with $E = -0.0867$ is the average over the six degenerate states. The parameters are $U = 0.3$, $t_{\text{cluster}} = -0.0324$ eV and $t' = 0$.

E	S	Deg.	P_d
-0.1116	0	1	0.39
-0.1062	1	1	0.30
-0.0941	2	1	0.12
-0.0867	1	6	0.17
-0.0764	0	9	0.11

more relevant for the large U situation, when all electrons on the cluster are localized. Since there are more levels, the energy splitting of the states is smaller. The difference in P_d is also smaller. At finite hopping to the bath and finite T , there is a finite occupation of many cluster states. For small T and large U , however, the lowest cluster state dominates. The lowest cluster state has RVB character⁶³ as discussed previously. This agrees with the results in Fig. 4, showing that the spin susceptibility $S(\pi, \pi)$ for large U behaves as expected for an RVB state. The value, $P_d = 0.39$ is slightly larger than the result found in Fig. 3 for large U for a cluster in a bath. This is reasonable, since there is also a slight mixture of excited states with smaller P_d for the embedded cluster.

IX. IMPLICATIONS OF A PSEUDOGAP

In the previous section we have seen that the pseudogap can be understood as corresponding to the break up of a (very short-range) $d_{x^2-y^2}$ singlet state. We can then reverse the statement and ask if a pseudogap implies the presence of a state with large superconductivity fluctuations. From the arguments above we would expect that this is not the case. In Sec. VI we argued that if the lowest cluster state is nondegenerate the system ought to show a pseudogap for sufficiently large U (in the first iteration). To test this we would then like to find a system where the lowest cluster state is nondegenerate, but

$P_{x^2-y^2}$ is small. We therefore consider a system where an antiferromagnetic field is applied to the cluster sites, but not to the bath. Thus we add

$$H_{\text{AF}} = \sum_i \gamma_i (n_{i\uparrow} - n_{i\downarrow}), \quad (62)$$

to the Hamiltonian in Eq. (1). Here $\gamma_i = \gamma$ if i belongs to one sublattice and $\gamma_i = -\gamma$ otherwise. We expect the field to be bad for $x^2 - y^2$ pairing. We have chosen a small value of $\gamma = 0.1t = 0.004$ eV. For $U = 0$ this has a very small effect on the solution for the $N_c = 8$ cluster.

In Fig. 32 we show spectra obtained for intermediate U . Since the system is not homogeneous, the spectra have been calculated from the Fourier transform of the spatial cluster Green's function. This gives the average spectrum over the patches around $\mathbf{K} = (\pi, 0)$ and $(\pi/2, \pi/2)$. In the limit $U = 0$ and $\gamma = 0$, this approach would give the density of states over the patches around $\mathbf{K} = (\pi, 0)$ and $(\pi/2, \pi/2)$. In particular the spectrum around $\mathbf{K} = (\pi/2, \pi/2)$ is therefore much broader than for other spectra in this paper. Those other spectra were calculated from Eq. (10), and the spectra would just consist of a δ -function in the limit $U = 0$ and $\gamma = 0$. It is then not surprising that the $(\pi/2, \pi/2)$ spectrum is rather broad. The interesting aspect is that for $U = 0.20$ eV the $(\pi, 0)$ spectrum shows a pseudogap, while the $(\pi/2, \pi/2)$ spectrum does not. For $U = 0.25$ eV both spectra show a pseudogap. For $U = 0.20$ eV and $\gamma = 0.004$ eV, the expectation value of the $d_{x^2-y^2}$ pairing operator is only 0.04 and for $U = 0.25$ it is 0.05. For $\gamma = 0$ a pseudogap forms for $U \sim 0.30$ eV (in the first iteration). The corresponding expectation value of the pairing operator is then 0.18. Thus the pseudogap is formed for $\gamma = 0.004$ eV although there are almost no superconductivity correlations in the system. This is then consistent with the arguments in Sec. VI that a nondegenerate lowest cluster state leads to a pseudogap.

X. CONCLUSIONS

Angular resolved photoemission spectra (ARPES) on cuprates show a pseudogap^{1,10} in the antinodal direction around the antinodal [$\mathbf{k} = (\pi, 0)$] point and a peak around the nodal [$\mathbf{k} = (\pi/2, \pi/2)$] point in a broad region of their phase diagram. The layered organic superconductors also show evidence for a pseudogap in susceptibility and $1/T_1 T$ -NMR experiments¹¹⁻¹³. Although the Mott transition in the cuprates is driven by doping whereas in the half-filled organics κ -(BEDT-TTF)₂X it is driven by external pressure, the pseudogap phenomenon appears to be similar in both systems suggesting a common origin.¹⁶

A pseudogap in the many-body spectral function is found in the DCA for the Hubbard model consistent with ARPES experiments on cuprates and previous works.¹⁹⁻²⁵ In order to understand the origin of the pseudogap within DCA we have singled out the following key

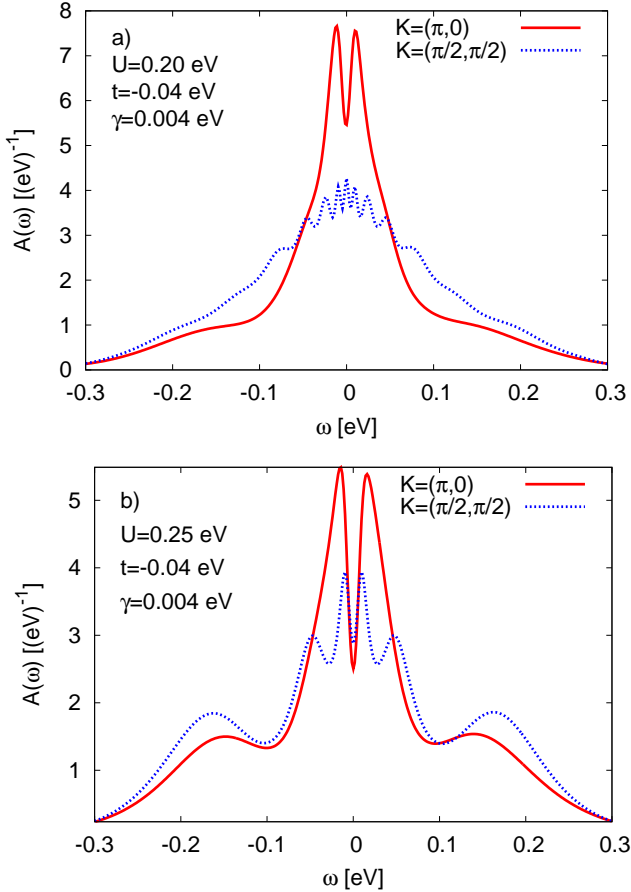


FIG. 32. Spectra for a model including the antiferromagnetic potential [Eq. (62)] on the cluster. A pseudogap is formed in the $(\pi, 0)$ channel but not in the $(\pi/2, \pi/2)$ channel for $U = 0.2$ eV, although the superconductivity fluctuations are strongly suppressed. The parameters are $t = -0.04$ eV, $t' = 0$, $\gamma = 0.004$ eV and $T = 38.4$ K.

ingredients: (i) Different bath-cluster couplings around antinodal and nodal points. (ii) The internal electronic structure of the cluster is crucial. This gives rise to an important competition between Kondo-like states and localization on the cluster. (iii) The ground state of the isolated cluster should be non-degenerate. Degenerate cluster ground states can lead to a Kondo peak in the spectra instead of a pseudogap.

The spectra of isolated clusters with $N_c = 8$ or 16 sites do not show any signs of the pseudogap observed in DCA, *i. e.* the spectra at the $(\pi, 0)$ and $(\pi/2, \pi/2)$ points obtained from ED are the same due to the special symmetries for these clusters. The absence of the pseudogap on small isolated clusters indicates that the pseudogap found in DCA is related to the much weaker coupling to the bath of the $(\pi, 0)$ than $(\pi/2, \pi/2)$ sector. In fact, we have shown that if the baths are switched the pseudogap occurs at $(\pi/2, \pi/2)$ instead of $(\pi, 0)$.

While single-site DMFT calculations require self-consistency to produce a gap, already first iteration DCA

calculations with clusters can give a pseudogap. This shows that the feedback effect on the bath is not necessary for the pseudogap opening in the DCA. This is due to the internal structure of the cluster and the formation of a nondegenerate localized state on the cluster, due to important correlations between the $(\pi, 0)$ and $(0, \pi)$ sectors, missing in single-site DMFT calculations. It is then important to understand the influence of the internal structure of the cluster on the pseudogap.

For this purpose, we have analyzed the ground state wavefunctions of isolated clusters. The ground state of the smaller $N_c = 4, 8$ isolated clusters is a short range NN-RVB state which can be expressed as linear combinations of configurations with doubly occupied $(\pi, 0)/(0, \pi)$ and $(\pm\pi/2, \pm\pi/2)$ sectors. These correlations are found to dominate in the large- U limit of DCA calculations, when the cluster is effectively decoupled from the bath. They are also present in the $(\pi, 0)/(0, \pi)$ sector at smaller U , in the pseudogap regime, indicating the importance of these characteristic cluster correlations for pseudogap formation.

We have devised a four-level model which contains the essential ingredients for describing the pseudogap observed in DCA for $N_c = 4$. The model includes $(\pi, 0)$ and $(0, \pi)$ levels on the cluster, each coupling to one bath level. With appropriate parameters, it simulates the non-degenerate singlet ground state and the low energy spectra of the $N_c = 4$ isolated cluster. We find that at small values of U each cluster level forms a Kondo-like state with its corresponding bath level. As U is increased, it becomes favorable to instead couple the $(\pi, 0)$ and $(0, \pi)$ levels to each other, forming a RVB singlet on an $N_c = 4$ cluster, and opening up a pseudogap. This competition between Kondo and cluster RVB state formation is crucial for the physics. We show that the characteristic correlations found in the four-level model for the $(\pi, 0)$ and $(0, \pi)$ levels also happen for DCA calculations with $N_c = 4$ and 8 clusters. For $N_c = 8$ calculations, the $(\pm\pi/2, \pm\pi/2)$ form Kondo-like states with the bath up to larger values of U , due to the stronger cluster-bath coupling in this channel.

For a particular choice of parameters of the four-level model, the isolated cluster has a triplet ground-state. Then the model has a Kondo state even for large values of U and no proper pseudogap is formed. This shows the importance of the lowest isolated cluster state being nondegenerate. Similar work has been done having alkali-doped fullerenes in mind.^{50,52,53}

The suppression of density of states at the Fermi level leading to the pseudogap observed in DCA and in the four-level model can be understood in terms of destructive interference processes. In the weakly coupled cluster-bath limit, $U/|V| \gg 1$, destructive interference can be captured for an infinite bath assuming that the lowest cluster state is non-degenerate. In photoemission, intensity at the Fermi energy corresponds to transitions to final states where cluster neutral configurations dominate. This can happen in essentially two ways. One way con-

sists of removing an electron from the cluster when an extra electron has hopped from the bath into the cluster, while the other involves the removal of an electron directly from the neutral cluster, followed by the hopping of a bath electron into the cluster. In both ways the system can reach the same final state in which the cluster is in a neutral state and the bath is left with a hole at the Fermi energy. Due to the negative interference between these two processes the spectral weight of the photoemission process is suppressed at the Fermi energy. This is in contrast to the case in which the the lowest state of the cluster is degenerate. As an example, we analyzed the degenerate impurity Anderson model in the large degeneracy N_f limit. In this case spin-flip terms become important. These terms interfere constructively with one of the paths important for the nondegenerate case, while the other path is of lower order in $(1/N_f)$. This leads to a peak at the Fermi energy.

There is a strong gain in correlation energy when both the $(\pi, 0)$ and $(\pm\pi/2, \pm\pi/2)$ sectors are allowed to localize simultaneously. This gives a strong tendency for all electrons in the cluster to localize simultaneously, leading to a common (pseudo)gap. This is counteracted by the large difference (factor 3-4) in the cluster-bath coupling for the $(\pi, 0)$ and $(\pm\pi/2, \pm\pi/2)$ sectors. As a result the pseudogap opens up for a smaller U for the $(\pi, 0)$ sector. However, the difference in U at which the pseudogap opens up in the two sectors is smaller than the difference in cluster-bath coupling, indicating the importance of the correlation between the $(\pi, 0)$ and $(\pm\pi/2, \pm\pi/2)$ sectors.

The pseudogap occurs close to the Mott transition in a parameter region in which short range d -wave singlet formation is found to be substantial. When an electron is emitted in the photoemission process it is energetically favorable for an electron in the bath to hop into the cluster. Since the lowest ground state of the neutral cluster has negligible spectral weight due to destructive interference effects, most of the weight will concentrate on excited states characterizing the flanks of the pseudogap. These excited states have suppressed d -wave correlations so that we can relate the pseudogap with the breaking of very short range d -wave pairs. However, we have also found that the observation of a pseudogap does not imply in general the existence of preformed d -wave pairs. We have constructed a model where such fluctuations are strongly suppressed, but still find a pseudogap, provided that the lowest state of the isolated cluster is nondegenerate.

Geometrical frustration has an important effect on the internal level structure of the isolated cluster. At $t'/t \sim 0.7$ there is a crossing of many-electron states, leading to a change of the cluster character. Interestingly, the κ -(BEDT-TTF)₂X family of organic superconductors displays a change from an antiferromagnetic (X=Cu[N(CN)₂]Cl) Mott insulator to a spin liquid Mott insulator (X=Cu₂(CN)₃) with⁵⁵ the ratios $t'/t \sim 0.4-0.5$ and $t'/t \sim 0.8-0.9$, respectively, straddling the ratio $t'/t \sim 0.7$ found above. In a model for the cuprates with,

$t' = -0.3t$, on a frustrated square lattice, the pseudogap is sensitive to the doping, being destroyed for electron doping but not for hole doping consistent with experiments on cuprates. This behavior can be understood from the effective enhancement of the Kondo coupling to the $(\pi, 0)$ bath as the chemical potential is raised. An interesting prediction is that in the organics due to the opposite positive t'/t ratio, the pseudogap would be enhanced for electron doping instead.

An important question arises in all DCA calculations. Are the small cluster calculations representative of the thermodynamic limit behavior? Several works have shown^{18,20,23} that the pseudogap is robust against increasing the cluster size up to $N_c = 16$. We have found that the pseudogap can be associated with short range singlet and antiferromagnetic correlations which characterize NN-RVB cluster states describing the ground state of small clusters ($N_c = 4, 8$). Cluster correlations on large clusters (up to $N_c = 64$) also display significant very short range d -wave singlet correlations and slowly decaying antiferromagnetic spin correlations. These correlations are consistent with RVB states including singlet bonds between sites further distant than nearest-neighbor sites. Hence, a mechanism in which Kondo and cluster singlet formation compete as in the smallest clusters discussed here can occur. Further work on larger clusters is needed to establish this important issue.

ACKNOWLEDGMENTS

JM acknowledges financial support from MINECO (MAT2012-37263-C02-01) and hospitality at Max-Planck-Institut für Festkörperforschung in Stuttgart during his stay there.

Appendix A: Coulomb integrals in four-level model

Here we discuss the Coulomb integrals used in the four level model for describing the $N_c = 4$ cluster. Table XIII shows results for the four lowest states of the isolated $N_c = 4$ cluster. We fit the parameters in the model to the three lowest levels, using the results in Eq. (34). These parameters are shown in Table XIII. We use the approximate parameterization $\Delta U = 0.03U$ and $K = 0.1U$, appropriate for intermediate values of U .

Normally $U_{xx} > U_{xy}$. However, due to the short range of the Hubbard interaction $U_{xx} = U_{xy}$. Furthermore, the interaction with the levels for $\mathbf{k} = (0, 0)$ and (π, π) cannot be neglected. This lowers the energies E_{1-} and E_{1+} more than E_{2-} and E_{2+} . We describe this by putting $U_{xx} < U_{xy}$ and by adjusting K .

The reason for these effects is illustrated in Fig 33. Due to the Coulomb interaction, configurations e) and f) couple to a) and b) with the same sign and strength. These then lower E_{1+} but not E_{1-} . Instead, configurations g) and h) couple to a) and b) with opposite signs, due to the

TABLE XIII. Eigenvalues E_i for a four-site Hubbard model with the parameters U and t . The parameters $U_{xx} = U - \Delta U$, $U_{xy} = U + \Delta U$ and K are fitted to the three lowest levels. While the three lowest states correspond to the three lowest states in Eq. (34), the fourth state is of different character than the fourth state in Eq. (34) for these values of U and t .

U	t	E_1	E_2	E_3	E_4	ΔU	K
0.25	-0.050	-0.0922	-0.0757	-0.0422	-0.0351	0.0083	0.0250
0.25	-0.030	-0.0383	-0.0285	-0.0148	-0.0137	0.0049	0.0118

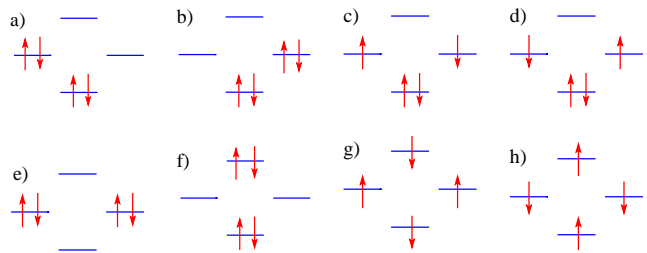


FIG. 33. Important configurations for the four-site cluster. The linear combinations of states a) and b) form the lowest and third lowest eigenstates, $|1-\rangle$ and $|1+\rangle$, respectively.

Fermion minus sign and an odd reordering of electrons. They then lower E_{1-} but not E_{1+} . These couplings are particularly efficient, since the same configuration couples to both a) and b). The two couplings are then added before the sum is squared. There are additional configurations coupling to a) and b), but then only to one or the other and therefore less efficiently. In contrast, no configuration couples to both c) and d). This then makes the coupling to c) and d) less efficient. Furthermore, fewer configurations couple to c) and d). Both these facts lead to a larger lowering of E_{1-} and E_{1+} than for E_{2-} and E_{2+} . We describe this by making $U_{xx} < U_{xy}$.

- ¹ A. G. Loeser, Z.-X. Shen, D. S. Dessau, D. S. Marshall, C. H. Park, P. Fournier, and A. Kapitulnik, *Science* **273**, 325 (1996); H. Ding, T. Yokoya, J. C. Campuzano, T. Takahashi, M. Randeria, M. R. Norman, T. Mochiku, K. Kadowaki, and J. Giapintzakis, *Nature (London)*, **382**, 51 (1996); M. R. Norman, H. Ding, M. Randeria, J. C. Campuzano, T. Yokoya, T. Takahashi, T. Mochiku, K. Kadowaki, P. Guptasarma, and D. G. Hinks, *Nature (London)*, **392**, 157 (1998); D. Damascelli, Z. Hussain, and Z.-X. Shen, *Rev. Mod. Phys.* **75**, 473 (2003).
- ² N. F. Mott, *Metal Insulator Transitions* (Taylor and Francis, London, 1990).
- ³ M. Imada, A. Fujimori, and Y. Tokura, *Rev. Mod. Phys.* **70**, 1039 (1998).
- ⁴ W. W. Warren, Jr., R. E. Walstedt, G. F. Brennert, R. J. Cava, R. Tyco, R. F. Bell, and G. Dabbagh, *Phys. Rev. Lett.* **62**, 1193 (1989).
- ⁵ H. Alloul, T. Ohno, and P. Mendels, *Phys. Rev. Lett.* **63**, 1700 (1989).
- ⁶ T. Ito, K. Takenaka, and S. Uchida, *Phys. Rev. Lett.* **70**, 3995 (1993).
- ⁷ R. Nemeschek, M. Opel, C. Hoffmann, P. F. Müller, R. Hackl, H. Berger, L. Forro, A. Erb, and E. Walker, *Phys. Rev. Lett.* **78**, 4837 (1997); X. K. Chen, J. G. Naeini, K. C. Hewitt, J. C. Irwin, R. Liang, and W. N. Hardy, *Phys. Rev. B* **56**, R513 (1997).
- ⁸ Ch. Renner, B. Rewaz, J.-Y. Genoud, K. Kadowaki, and O. Fischer, *Phys. Rev. Lett.* **80**, 149 (1998).
- ⁹ Y. Kohsaka, C. Taylor, P. Wahl, A. Schmidt, J. Lee, K. Fujita, J. W. Alldredge, K. McElroy, J. Lee, H. Eisaki, S. Uchida, D.-H. Lee, and J. C. Davis,
- ¹⁰ T. Timusk and B. Statt, *Rep. Prog. Phys.* **62**, 61 (1999). *Nature (London)* **454**, 1072 (2008).
- ¹¹ K. Kanoda, *Jour. Phys. Soc. Jpn.*, **75**, 051007 (2006).
- ¹² A. Kawamoto, K. Miyagawa, and K. Kanoda, *Phys. Rev. B* **55**, 14140 (1997); K. Miyagawa, *et. al.*, *Phys. Rev. Lett.* **89**, 017003 (2002).
- ¹³ H. Mayaffre *et. al.*, *Europhys. Lett.* **28**, 205 (1994).
- ¹⁴ Y. Shimizu, *et. al.* *Phys. Rev. Lett.* **91**, 107001 (2003).
- ¹⁵ Y. Kurosaki, *et. al.* *Phys. Rev. Lett.* **95**, 177001 (2005).
- ¹⁶ R. H. McKenzie, *Science* **278**, 820 (1997).
- ¹⁷ K. Haule, A. Rosch, J. Kroha, and P. Wölfle, *Phys. Rev. Lett.* **89**, 236402 (2002); *Phys. Rev. B* **68**, 155119 (2003).
- ¹⁸ T. Maier, M. Jarrell, T. Pruschke, and M. H. Hettler, *Rev. Mod. Phys.* **77**, 1027 (2005).
- ¹⁹ M. Civelli, M. Capone, S. S. Kancharla, O. Parcollet, and G. Kotliar *Phys. Rev. Lett.* **95**, 106402 (2005).
- ²⁰ A. Macridin, M. Jarrell, T. Maier, P.R.C. Kent, and E. D’Azevedo, *Phys. Rev. Lett.* **97**, 036401 (2006).
- ²¹ B. Kyung, S. S. Kancharla, D. Senéchal, and A.-M.S. Tremblay, M. Civelli, and G. Kotliar, *Phys. Rev. B* **73**, 165114 (2006); B. Kuyang and A. M. S. Tremblay, *Phys. Rev. Lett.* **97**, 046401 (2006).
- ²² M. Ferrero, P. S. Cornaglia, L. De Leo, O. Parcollet, G. Kotliar, and A. Georges, *Phys. Rev. B* **80**, 064501 (2009).
- ²³ P. Werner, E. Gull, O. Parcollet, and A.J. Millis, *Phys. Rev. B* **80**, 045120 (2009); E. Gull, O. Parcollet, P. Werner, and A.J. Millis, *Phys. Rev. B* **80**, 245102 (2009); N. Lin, E. Gull, and A.J. Millis, *Phys. Rev. B* **82**, 045104 (2010); E. Gull, M. Ferrero, O. Parcollet, A. Georges and A. J. Mil-

- lis, Phys. Rev. B **82**, 155101 (2010).
- ²⁴ A. Liebsch and N.-H. Tong, Phys. Rev. B **80**, 165126 (2009).
- ²⁵ G. Sordi, P. Semon, K. Haule, and A.-M.S. Tremblay, Phys. Rev. Lett. **108**, 216401 (2012).
- ²⁶ V.J. Emery and S.A. Kivelson, Nature **374**, 434 (1995).
- ²⁷ Z. A. Xu, N. P. Ong, Y. Wang T. Kakeshita and S. Uchida, Nature **406**, 486 (2000).
- ²⁸ Y. Kosaka, T. Hanaguri, M. Azuma, M. Takano, J. C. Davis, and H. Takagi, Nature Physics **8**, 534 (2012).
- ²⁹ Y. Wang, L. Li, M. J. Naughton, G. D. Gu, S. Uchida, and N. P. Ong, Phys. Rev. Lett. **95**, 247002 (2005).
- ³⁰ E. Gull, O. Parcollet and A.J. Millis, Phys. Rev. Lett. **110**, 216405 (2013).
- ³¹ H. Morita, S. Watanabe, and M. Imada, Jour. Phys. Soc. Jpn. **71**, 2109 (2002).
- ³² T. Yoshioka, A. Koga and N. Kawakami, Phys. Rev. Lett. **103**, 036401 (2009).
- ³³ P. Sahebsara and D. Senechal, Phys. Rev. Lett. **97**, 257004 (2006); **100**, 136402 (2008).
- ³⁴ O. Parcollet, G. Brioli, and G. Kotliar, Phys. Rev. Lett. **92**, 226402 (2004).
- ³⁵ T. Ohashi, T. Momoi, H. Tsunetsugu, and N. Kawakami, Phys. Rev. Lett. **100**, 076402 (2008).
- ³⁶ A. Liebsch, H. Ishida, and J. Merino Phys. Rev. B **79**, 195108 (2009).
- ³⁷ J. Kokalj, and R. H. McKenzie, Phys. Rev. Lett. **110**, 206402 (2013).
- ³⁸ J. Kang, S. L. Yu, T. Xiang, and J.-X. Li, Phys. Rev. B **84**, 064520 (2011).
- ³⁹ W. Metzner and D. Vollhardt, Phys. Rev. Lett. **62**, 324 (1989); M. Jarrell, Phys. Rev. Lett. **69**, 168 (1992); A. Georges, G. Kotliar, W. Krauth, M.J. Rozenberg, Rev. Mod. Phys. **68**, 13 (1996).
- ⁴⁰ A. Georges, G. Kotliar, W. Krauth, and M. J. Rozenberg, Rev. Mod. Phys. **68**, 13 (1996).
- ⁴¹ G. Kotliar, S. Y. Savrasov, K. Haule, V. S. Oudovenko, O. Parcollet, and C. A. Marianetti, Rev. Mod. Phys. **78**, 865 (2006).
- ⁴² J. Merino and R. H. McKenzie, Phys. Rev. B **61**, 7996 (2000).
- ⁴³ P. Limelette, P. Wzietek, S. Florens, A. Georges, T. A. Costi, C. Pasquier, D. Jerome, C. Meziere, and P. Batail, Phys. Rev. Lett. **91**, 016401 (2003).
- ⁴⁴ J. Merino, M. Dumm, N. Drichko, M. Dressel, and R. H. McKenzie, Phys. Rev. Lett. **100**, 086404 (2008).
- ⁴⁵ K. Frikach, M. Poirier, M. Castonguay, and K. D. Truong, Phys. Rev. B **61**, R6491 (2000); D. Fournier, M. Poirier, M. Castonguay, and K. D. Truong, Phys. Rev. Lett. **90**, 127002 (2003); J. Merino and R. H. McKenzie, Phys. Rev. B **62**, 16442 (2000); S. R. Hassan, A. Georges, and H. R. Krishnamurthy, Phys. Rev. Lett. **94**, 036402 (2005).
- ⁴⁶ R. C. Yu, J. M. Williams, H. H. Wang, J. E. Thompson, A. M. Kini, K. D. Carlson, J. Ren, M. H. Whangbo, and P. M. Chaikin, Phys. Rev. B **44**, 6932 (1991).
- ⁴⁷ B. J. Powell, E. Yusuf, and R. H. McKenzie, Phys. Rev. B **80**, 054505 (2009).
- ⁴⁸ H. Park, K. Haule, and G. Kotliar, Phys. Rev. Lett. **101**, 186403 (2008).
- ⁴⁹ F. Kagawa, T. Itou, K. Miyagawa, and K. Kanoda, Phys. Rev. B **69**, 064511 (2004).
- ⁵⁰ M. Fabrizio, A. F. Ho, L. De Leo, and G. E. Santoro, Phys. Rev. Lett. **91** 246402 (2003); L. De Leo, M. Fabrizio, PRB **69**, 245114 (2004); PRL **94**, 236401 (2005).
- ⁵¹ A. Liebsch, H. Ishida, and J. Merino, Phys. Rev. B **78**, 165123 (2008).
- ⁵² M. Ferrero, L. De Leo, P. Lecheminant and M. Fabrizio, J. Physics: Cond. Matt. **19**, 433201 (2007).
- ⁵³ M. Capone, M. Fabrizio, C. Castellani, E. Tosatti, Rev. Mod. Phys. **81**, 943 (2009); M. Capone, M. Fabrizio, C. Castellani, E. Tosatti, Phys. Rev. Lett. **81**, 943 (2004).
- ⁵⁴ J. Merino and O. Gunnarsson, J. Physics: Cond. Matt. **25**, 052201 (2013).
- ⁵⁵ H. C. Kandpal, I Opahle, Y.-Z. Zhang, H. O. Jeschke, and R. Valenti, PRL **103**, 067004 (2009); W. Y. Ching, Y.-N. Xu Y. C. Jean, and Y. Lou, PRB **55** 2780 (1997); J. Merino and R. H. McKenzie, PRB **62**, 2416 (2000);
- ⁵⁶ J. Jaklic and P. Prelovsek, Adv. Phys. **49**, 1 (2000).
- ⁵⁷ D.D. Betts, H.Q. Lin, and J.S. Flynn, Can. J. Phys. **77**, 353 (1999).
- ⁵⁸ E. Koch, G. Sangiovanni, and O. Gunnarsson, Phys. Rev. B **78**, 115102 (2008).
- ⁵⁹ M. Jarrell and J.E. Gubernatis, Phys. Rep. **269**, 133 (1996).
- ⁶⁰ S. Liang, B. Doucot, and P. W. Anderson, Phys. Rev. Lett. **61**, 365 (1988).
- ⁶¹ W. Marshall, Proc. Roy. Soc. (London), **A232**, 48 (1955).
- ⁶² P. Fazekas, *Electron Correlation and Magnetism*, World Scientific. (2003). T
- ⁶³ S. Tang and H.Q. Lin, Phys. Rev. B **38**, 6863 (1988).
- ⁶⁴ J Oitmaa and D. D. Betts, Canadian Journal of Physics, **56**, 897 (1978).
- ⁶⁵ M. J. Rozenberg, R. Chitra, and G. Kotliar, Phys. Rev. Lett. **83**, 3498 (1999).
- ⁶⁶ B Kyung, G. Kotliar, and A.-M. S. Tremblay, Phys. Rev. B **73**, 205106 (2006).
- ⁶⁷ E. Dagotto, R. Joynt, A. Moreo, S. Bacci, and E. Gagliano, Phys. Rev. B **41**, 9049 (1990).
- ⁶⁸ O. Gunnarsson and K. Schönhammer, Phys. Rev. B **28**, 4315 (1983).
- ⁶⁹ W.-D. Schneider, B. Delley, E. Wuilloud, J.-M. Imer, and Y. Baer, Phys. Rev. B **32**, 6819 (1985).
- ⁷⁰ A. Liebsch, Phys. Rev. Lett. **22** 226401 (2003).
- ⁷¹ A. Koga, N. Kawakami, T. M. Rice, and M. Sigrist, Phys. Rev. Lett. **92** 216402 (2004).
- ⁷² L. de' Medici, S. R. Hassan, M. Capone, and X. Dai, Phys. Rev. Lett. **102**, 126401 (2009); L. de' Medici, Phys. Rev. B **83**, 205112 (2011).
- ⁷³ P. Werner, E. Gull, M. Troyer, and A. J. Millis, Phys. Rev. Lett. **101**, 166405 (2008).
- ⁷⁴ S. Biermann, L. de' Medici, and A. Georges, Phys. Rev. Lett. **95**, 206401 (2005).
- ⁷⁵ N. P. Armitage, F. Ronning, D. H. Lu, C. Kim, A. Damascelli, K. M. Shen, D. L. Feng, H. Esaki, Z. X. Shen, P. K. Mang, N. Kaneko, M. Greven, Y. Onose, Y. Taguchi, and Y. Tokura, Phys. Rev. Lett. **88**, 257001 (2002).